
Article:
Laagland, L.T. orcid.org/0000-0002-4456-6167, Salzer, E. orcid.org/0000-0001-8711-4243, Fabra, G.T. et al. (17 more authors) (2026) A bioactive hydrogel harnessing the regenerative potential of notochordal cells serves as instructive cell carrier for nucleus pulposus repair. Biomaterials, 328. 123895. ISSN: 0142-9612

https://doi.org/10.1016/j.biomaterials.2025.123895

A bioactive hydrogel harnessing the regenerative potential of notochordal cells serves as instructive cell carrier for nucleus pulposus repair

[1]Lisanne T. Laagland[a, b] (l.t.laagland@uu.nl), [1,3]Elias Salzer[c] (e.salzer@erasmusmc.nl), [1]Georgina Targa Fabra[d] (georgina.targa1@gmail.com), [3]Xiaole Tong[a, b] (x.tong@erasmus.nl), Deepani W. L. Poramba-Liyanage[a, b] (deepsliyanage@gmail.com), Julie Warin[e] (julie.warin@etu.univ-nantes.fr), Kieran Joyce[d] (kieran.joyce@universityofgalway.ie), Joseph Snuggs[f] (j.snuggs@sheffield.ac.uk), Frank M. Riemers[a, b] (f.m.riemers@uu.nl), Lizette Utomo[a, b] (l.utomo@uu.nl), Seyed A. Kamali[a] (s.a.kamali@uu.nl), Tara C. Schmitz[c] (tara.schmitz@outlook.de), Noemy S. Vergara Vera[b] (n.s.vergara.vera@tue.nl), Christine L. Le Maitre[f] (c.lemaitre@sheffield.ac.uk), Benjamin Gantenbein[g, h] (benjamin.gantenbein@unibe.ch), Björn P. Meij[a] (b.p.meij@uu.nl), Anne Camus[e] (anne.camus@univ-nantes.fr), [2]Keita Ito[c] (K.Ito@tue.nl), [2*]Abhay Pandit[d], [2*]Marianna A. Tryfonidou[a, b]

[a]Utrecht University, Yalelaan 108, Utrecht, The Netherlands; [b]Regenerative Medicine Center Utrecht, The Netherlands; [c]Eindhoven University of Technology, Eindhoven, The Netherlands; [d]CÚRAM, Research Ireland Centre for Medical Devices, University of Galway, Galway, Ireland; [e]Nantes University , Oniris, CHU Nantes, Inserm, Regenerative Medicine and Skeleton, RMeS, UMR 1229, Nantes, France; [f]University of Sheffield, Sheffield, United Kingdom; [g]Tissue Engineering for Orthopaedics & Mechanobiology, Bone & Joint Program, Department for BioMedical Research (DBMR), Faculty of Medicine, University of Bern, Bern, Switzerland; [h]Department of Orthopaedic Surgery & Traumatology, Inselspital, Bern University Hospital, Faculty of Medicine, University of Bern, Bern, Switzerland

[1]Contributed equally
[2]Contributed equally
[3]Current affiliation: Department of Orthopaedics and Sports Medicine, Erasmus MC, University Medical Centre Rotterdam, The Netherlands.

[*]Corresponding authors:
- M. A. Tryfonidou
  Address: Yalelaan 108, 3584 CM, Utrecht, The Netherlands
  Email: M.A.Tryfonidou@uu.nl
  Tel: +31302539411
- A. Pandit
  Address : University Rd, Galway, Ireland
  Email: abhay.pandit@universityofgalway.ie
  Tel: +35391524411

Abstract

Natural biomatrices are popular owing to their ability to mimic tissue-specific biological properties. These properties are crucial for the intervertebral disc, a particularly demanding tissue whose degeneration is a major cause of chronic lower back pain. Degeneration starting within the core of the disc, the nucleus pulposus (NP), is marked by the loss of notochordal cells (NCs) and associated-healthy extracellular matrix. The regulative potential of the NC-secretome was exploited through a PEG-based hydrogel formulated with decellularized porcine notochordal cell matrix (dNCM). Even under conditions which mimic the degenerate niche, the hydrogel supported maintenance of the native porcine NC phenotype, well-known for the difficulty in preserving their vacuolated phenotype. dNCM-PEG hydrogel carrying human mesendodermal progenitors (hMEPCs; iPSC-derived and capable of differentiating into NCs), was injected into NP explants with enzymatically induced matrix degradation and subjected to dynamical loading. hMEPCs engrafted successfully and a healthy disc cell phenotype was observed. Injection of dNCM+hMEPCs into degenerated discs in a pilot experimental dog study indicated that ~7% of the 0.5 million hMEPCs engrafted. Single cell RNAseq analysis showed over 30% of the engrafted and recovered hMEPCs co-expressed *Collagen Type II* and *Aggrecan* consistent with a functional phenotype. No tumorigenic or systemic immunogenic side effects were observed. At the tissue level, TBXT expression, as well as matrix quality, were enhanced in the treated degenerate disc tissues. Together, this study highlights the translational potential of combining cell-based therapies with a bioactive material containing part of the NC secretome, warranting further development and validation.

Keywords: bioactive materials, induced pluripotent stem cells, bioreactors, explant culture, regeneration, low back pain

1. Introduction

A common cause for chronic low back pain is degeneration of the intervertebral disc (IVD), with an estimation of > 40 million patients worldwide [1, 2]. This degenerative process often starts within the core of the IVD, the nucleus pulposus (NP), and is characterized by cell depletion and extracellular matrix (ECM) degradation [3]. In IVD regeneration obstacles remain in implementing cell-based therapies. First, the environment of the degenerated IVD is harsh for cells to survive, as it is avascular with a limited nutrient supply and waste removal, resulting in low oxygen, glucose, and pH levels [4, 5]. Additionally, IVDs are subjected to dynamic loading, which imposes significant metabolic demands on the transplanted cells in this nutrient-limited environment [6]. These circumstances lead to poor cell survival, and thus only short-term and minimal clinical improvement after the injection of mesenchymal stromal cells (MSC) [7, 8]. Hence, while biomaterials serve as cell carriers minimizing the

risk of cell leakage upon intra-discal injection, they also need to provide the appropriate microenvironment allowing cells to thrive and fulfil regenerative roles, for example, production of healthy ECM rich in aggrecan and collagen type II [9] and/or stimulation of resident cells to deposit healthy ECM. In this context, bioactive biomaterials may offer a promising approach for an emerging tissue-specific cell type, the notochordal cell (NC), which has been shown to possess distinct regenerative abilities (reviewed by Bach *et al*. 2022) [10] for IVD degeneration.

Large vacuolated NCs reside within the developing human disc and by about 10 years of age, they disappear and are replaced by smaller non-vacuolated NP cells (NPCs) [11, 12]. NCs have a higher proteoglycan production capacity than NPCs [13, 14] and play an essential role in IVD homeostasis. They produce secretory products that can regulate NPCs toward a healthy state in multiple species [15]. Porcine NC-derived matrix (NCM) and its decellularized version (dNCM) [16] stimulate NPCs to produce healthy ECM and proliferate *in vitro* [17, 18], exert anti-inflammatory effects [17, 18], and have promising regenerative effects *in vivo* on degenerated canine IVDs [17]. (d)NCM may act as an 'instructive matrix'—similar to bovine derived demineralized bone matrix in bone regeneration [19] by providing ECM cues and locally releasing growth factors. Consequently, intradiscal injection of (d)NCM could represent a promising regenerative therapy for IVD disease, potentially bypassing the complex task of identifying the specific bioactive substances secreted by NCs. Based on this and many other studies, NCs and their secretome-containing ECM proteins and trophic factors, have received attention as potential sources for cell therapy to halt or reverse IVD degeneration [10].

The implementation of NC-based therapeutic approaches presents several challenges. Native NCs are scarcely available; humans do not maintain NCs beyond adolescence, resulting in considerable ethical challenges concerning the use of fetal NCs and/or NC-rich IVDs [20, 21]. Another key limitation of therapeutic approaches employing NCs is the preservation of their specific phenotype during isolation and expansion (reviewed by Williams *et al.* 2023) [22]. To overcome this, the field has shifted from native NCs to induced pluripotent stem cell (iPSC)-based technologies [23]. Human iPSC-derived mesendoderm progenitor cells (hMEPCs) have already shown potential to further differentiate into notochordal-like cells (NLCs) *in vitro* [24, 25] and are considered a promising alternative to native NCs for NP regeneration. However, achieving further differentiation of hMEPCs *in vitro* into mature NLCs has been challenging with studies reporting heterogeneous cell populations with only low percentages of NLC [24]. Purification of iPSC-derived NLCs requires the use of surface markers which have not been confirmed yet for their potency for purification and even then, this would remain a bottleneck in achieving sufficient yield of cells available for translational and clinical studies. Furthermore, NLCs developed *in vitro* [24-28] fail to further mature to ultimately mimic the considerable instructive and matrix-producing capacity of native NCs. The incorporation of natural substrates into biomaterials is

an attractive proposition to provide bioactive materials that interact with biological systems and may provide additional cues for differentiation of iPSCs [29]. Notably, NC-conditioned medium has been employed to differentiate mouse iPSCs that are positive for CD24, which is considered an NP cell progenitor marker [30], into NP-like cells that can synthesize matrix components similar to those of native NP [31]. In this context, dNCM containing naturally occurring bioactive ECM components may provide tissue-specific signaling cues to promote differentiation towards the NC-lineage over any growth factor supplementation [10, 29]. Furthermore, less stiff biomaterials, which may incorporate naturally derived components, are better carriers for optimal biological performance of injected cells [32]. This aligns with the softer biomechanical environment found in IVDs with NCs than in IVDs with NPCs [33-35].

To conclude, there is an unmet need for suitable bioactive materials that can both protect and guide the injected cells towards the NC lineage. Therefore, the goal of this study was to develop a bioactive dNCM-based hydrogel cross-linked with polyethylene glycol (PEG) which provides a supportive environment and serves as an instructive cell carrier (Figure 1). The protective capacity of the dNCM-PEG hydrogel was studied following encapsulation of native porcine NCs and exposing them to harsh degenerated IVD conditions, *that is*, low nutrient and oxygen levels. The instructive capacity was studied by determining the cell fate and regenerative effects of the bioactive and biodegradable dNCM-PEG hydrogel in combination with hMEPCs after injection into degenerated bovine NP explants. In this *ex vivo* model, early IVD degeneration and daily biomechanical loading were mimicked[6, 36] with 28 days follow-up [37] providing a clinically relevant IVD model as reviewed by Salzer *et al.* 2023 [38]. Finally, dNCM+hMEPCs was further evaluated in a pilot study using a well-established preclinical dog model of disc degeneration [17] by studying effects at tissue-level via biochemistry and at the cellular level through single-cell sequencing.

2. Material and Methods

If not stated otherwise, chemicals were purchased from Merck (St. Louis, USA).

2.1 Decellularized notochordal cell-derived matrix (dNCM) synthesis

In compliance with Dutch regulations, spines were obtained from less than 12-week-old piglets from the slaughterhouse. The NC-rich NP tissue, which can be easily discerned from the AF, was harvested aseptically, devitalized, and dehydrated using a freeze-dryer. Next, NCM was decellularized by a detergent-free protocol using Benzonase® Nuclease (70746-4)) treatment (200 U/mL) for 48 h at 37 °C on a roller mixer at 2 rpm and subsequently washed in saline, frozen, lyophilized, pulverized, and sterilized *via* UV irradiation before storage at -80 °C (Figure 1A) [16].

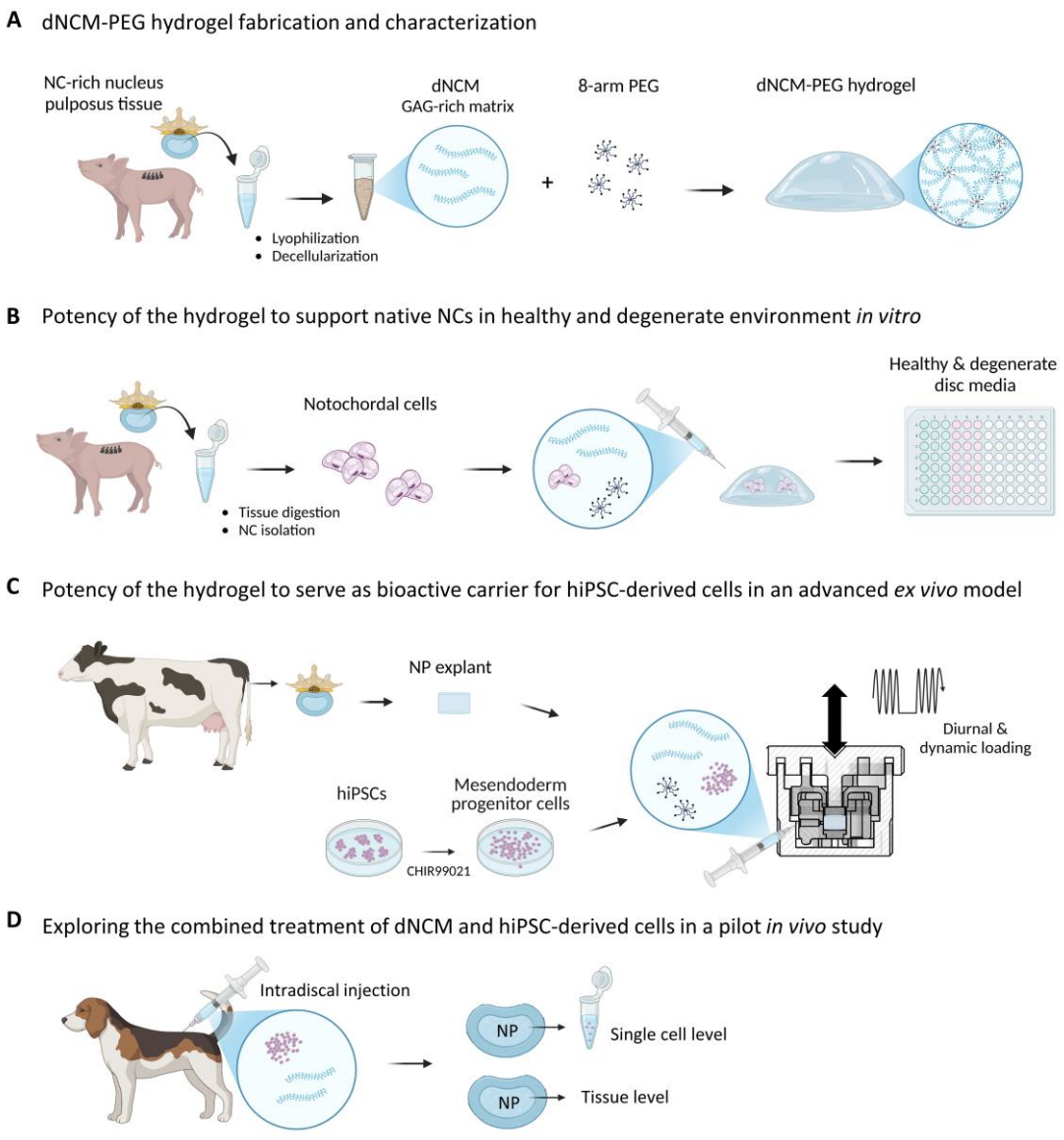

Figure 1: General set-up of the study. A hydrogel was fabricated based upon porcine-derived decellularized notochordal cell derived matrix (dNCM) crosslinked with 8-arm poly-ethylene glycol (PEG) (**A**). The potency of the dNCM-PEG hydrogel to support native notochordal cells (NCs) in a healthy and degenerate environment *in vitro* was tested (**B**). As a translational step, the potency of the injectable dNCM-PEG hydrogel to serve as bioactive carrier for human iPSC-derived cells in an advanced *ex vivo* model was investigated under diurnal and dynamic loading in bovine NP tissue explants (**C**), and the effect of dNCM+hMEPCs was further explored in an *in vivo* pilot study studying effects at NP tissue level, as well as by studying the effect on resident dog NPCs and hMEPCs. Here, non-crosslinked dNCM was used allowing for analysis through single cell RNAseq (**D**).

2.2 Fabrication of a dNCM-based poly-ethylene glycol (PEG) hydrogel

The hydrogel was fabricated via an amide reaction, which resulted in a highly stable covalent bond between the carboxyl groups of the glycosaminoglycan (GAG)-rich ECM in the dNCM and the NH_2 amine terminal of the PEG crosslinker (Figure 1A). dNCM was dissolved in 0.1 M 4-Morpholineethanesulfonic acid (MES) buffer pH 7.2 (M3671) and left overnight at 4 °C to dissolve fully. Subsequently, 4-(4,6-dimethoxy 1,3,5-triazin-2-yl)-4-methyl-morpholinium chloride (DMTMM; 348960050, Thermo Fisher, Waltham, Massachusetts, USA), dissolved in 0.1 M MES buffer, and was added to the dNCM to activate its carboxylic groups. Finally, 8-arm PEG amine (tripentaerythritol) and HCL Salt (8ARM(TP)-NH2HCL-20K, JenKem Technology, Plano, USA) were added and vortexed to ensure proper mixing of the gel solution. This 8-arm PEG derivative, with terminal amine groups promoted a more efficient cross-linking reaction compared to 4-arm PEG (Supplementary Figure 1A-C). The hydrogel contained a final concentration of 15 mg/mL dNCM, 21 mg/mL 8-arm PEG, and 15 mg/mL DMTMM. This concentration of dNCM was based on the predicted molar ratio of active sites for cross-linking and previous rheological tests with non-decellularized NCM (Supplementary Figure 1A-C), which showed that 15 mg/mL in a 2:1 ratio with 8-arm PEG was the highest concentration suitable for injection through a 27 G needle necessary for clinical application [39] and formation of a cross-linked hydrogel with the desired rheological properties. The mixed hydrogel formulation was incubated at 37 °C for 3 h to allow for polymerization (Supplementary Video 1).

2.3 Generation of human induced pluripotent stem cell-derived MEPCs

As human NCs are scarcely available, hiPSC-derived MEPCs could be a promising alternative cell source since they have already shown their potential to further differentiate towards NLCs[24, 25]. hMEPCs were generated following the method described by Warin *et al.* (2024)[24] with written consent from the human donors (approved by the ethical commission of the Canton of Bern, SwissEthics #2019-00097). In short, hiPSCs (hPSCreg Name: REGUi016-D 4F_PBMC_Sv190) were expanded on human rLaminin-521 (cat# 354221, Corning, NY, USA) -coated 6-well plates (Falcon, 353046, Corning, NY, USA) or chamber slides (80826, ibidi GmbH, Gräfelfing, Germany) for two days in mTeSR™1 medium (Stem Cell Technologies, Vancouver, Canada, 85851 batch #AG29793402 + supplement 85821 batch #1000068567, Vancouver, Canada) followed by 48 h culture in N2B27 media, containing DMEM-F12 (Gibco, 11330) with MEM non-essential amino acids 1% (Gibco, 1140), GlutaMAX 1% (Gibco, 35050), β-mercaptoethanol 0.01% (Gibco, 31350), N2 5% (Gibco, 17502048), B27 5% (Gibco, 17504044), and 1.25 mg/mL Bovine Serum Albumin (BSA) (Sigma Aldrich, A1595). This medium was supplemented with 3 µM CHIR99021 (cat# 1386, Axon Reston, USA) to commit the cells towards the mesendodermal identity (Figure 1C). The identity of these hMEPCs was confirmed by performing immunofluorescence (IF) on 4% paraformaldehyde fixed cells in chambers slides. The samples were then saturated and

permeabilized for 1 h at room temperature with 0.1% Triton and 3% BSA in phosphate buffered saline (PBS). Cells were incubated with primary antibodies (anti-TBXT [0.5 µg/mL; R&D Systems, af2085, Minneapolis, USA] and anti-FOXA2 [0.075µg/ml; Ozyme, 8186S, Saint-Cyr-l'École, France]) overnight at 4 °C in 1% BSA in PBS. After washing with PBS, incubation with secondary antibodies was performed using donkey anti-goat IgG (H+L) antibody (Alexa Fluor 488 conjugated, 2 µg/mL; Molecular Probes, A-cat# 11055, Thermo Fisher) or donkey anti-rabbit IgG (H+L) antibody (Alexa Fluor 594, 2 µg/mL; Molecular Probes A-21207, Thermo Fisher) for 1 h at room temperature in 1% BSA in PBS. After washing the secondary antibodies with PBS, the cells were counterstained with Hoechst 33258 pentahydrate (bis-benzimide) (2 µg/mL, H3569, Life Technologies) to visualize the nuclei and stored in CitiFluor™ AF1 (Electron Microscopy Sciences, #1179 70-25) at 4 °C. Confocal IF images were acquired using an LFOV FLIM Nikon® confocal microscope (Nikon, inc. Tokio, Japan). For each sample, three pictures were taken randomly within the well at 20 × magnification. Positive cells were quantified using the Volocity software (version 6.3, Quorum Technologies, San Jose, USA). These data confirmed the identity of the hMEPCs as 63% $TBXT^+/FOXA2^+$ cells (Supplementary Figure 2A, B). hMEPCs were dissociated using TryplE for 5 min at 37 °C, counted, and immediately used (referred to as "fresh") or frozen at 4×10^6 cells/ml in Cryostor® CS10 (Stem Cell Technologies, 100-1061), and stored in liquid nitrogen until further use.

2.4 Characterization of the dNCM-PEG hydrogel

To assess the swelling capacity of the dNCM-PEG formulation, it was first freeze-dried, and the initial dry weight (W_i) was measured. The hydrogel was incubated at 37 °C in either healthy or degenerate disc media developed previously (manuscript in preparation) to mimic different NP environments *in vivo* (see Table 1; Supplementary Table 1) [5, 40]. The final weight (W_f) of the gel was measured after 10 min, 30 min, 1 h, 2 h, 24 h, and 96 h, and the swelling capacity was calculated as a percentage increase using the following equation:

$$(W_f - W_i)/W_i * 100 \quad \text{Eqn 1}$$

To analyze the biomechanical properties, the storage and loss moduli of the dNCM-PEG hydrogel were determined. Since the presence of cells can influence the properties of the hydrogel these measurements were performed with encapsulated fresh hMEPCs in a concentration of 2×10^6 cells/mL corresponding with the intended application in our advanced *ex vivo* model (Figure 1C). Rheological measurements were performed using a MCR 501 Modular Compact Rheometer (Anton Paar, Austria). Briefly, the mixed hydrogel formulations were incubated at 37 °C for 3 h for polymerization and thereafter added to the plate at 37 °C. The rheometer was equipped with a circulating water bath to control the temperature. After a 5 min conditioning step, to ensure a normal force close to zero and

equilibrate the sample temperature, storage modulus (G') and loss modulus (G'') were determined by applying shear oscillations at a constant stress of 0.5 Pa and a frequency of 1 Hz for 5 min.

2.5 3D-encapsulation of porcine notochordal cells in dNCM-PEG hydrogel *in vitro*

Before investigating the potency of the hydrogel to serve as a cell carrier for the hMEPCs to protect them in the harsh IVD environment and further direct them towards the NC-lineage, we first analyzed to what extent the hydrogel supported the viability, vacuolated morphology, and phenotype of native NCs (Figure 1B). As human NCs are scarcely available, porcine NCs (pNCs) were used for this purpose. NP tissues were harvested from less than 12-week-old piglets (easily obtainable and rich in NCs[10]) and digested with 7 U/mL pronase (10165921001; Roche Diagnostics, Rotkreuz, Switzerland) for 30 min followed by overnight incubation with 125 U/mL collagenase II (LS004177; Worthington, Columbus, USA) on a roller mixer at 40 rpm at 37 °C. The following day, pNCs were seeded in the dNCM-PEG hydrogel formulation at a density of 4×10^6 cells/mL, corresponding to the higher end of the cell density of a human native NP ($2–4 \times 10^6$ cells/cm^3) [12] to enhance the insights on the cytocompatibility and cell supportive capacity of the hydrogel. Cells encapsulated in a volume of 50 µL were cultured for 14 days in low-adherence cell-repellent surface 96-well plates (650 970, CELLSTAR Greiner Bio-One, Frickenhausen, Germany) and maintained at 37 °C and 5% O_2 to mimic the hypoxic *in vivo* environment (considered tissue physioxia) [41]. To determine the cytocompatibility of the dNCM-PEG hydrogel and the ability to support the NC phenotype in a healthy and degenerate NP environment, different media compositions mimicking these conditions were used (Table 1) [5, 40]. The medium was refreshed every three days under normoxic conditions.

Table 1: Composition and properties of healthy and degenerate disc media [5, 40, 42]

Healthy	Degenerate
Low glucose DMEM	Low glucose DMEM
450 mOsm/kg	350 mOsm/kg
pH 7.1	pH 6.8
-	100 pg/mL IL-1β

2.5.1 Assessing pNC viability

To assess cell viability of the pNCs directly after encapsulation, images were obtained using a microscope (Leica TCS SP8 X, Leica, Germany) after whole-mount staining with Calcein-AM and Propidium Iodide. However, since cluster formation and the background signal of the hydrogel hampered proper quantification, the double-stranded (ds)DNA content of the pNCs was measured using the Qubit® dsDNA High Sensitivity Assay Kit (Invitrogen, Q32851, Thermo Fisher) according to the manufacturer's instructions to estimate the number of living cells on days 0, 7, and 14. The hydrogels were first digested by overnight incubation at 60 °C in 300 µL papain digestion solution (pH

6, 200 mM H_2NaPO_4*2 H_2O (21254, Boom B.V., Meppel, the Netherlands), 10 mM EDTA (100944, Merck Millipore, Amsterdam, the Netherlands), 10 mM cysteine HCl (C7880, Sigma-Aldrich, Saint Louis, USA), and 10 mM papain (P3125, Sigma-Aldrich).

2.5.2 Morphology and phenotype of the pNCs after encapsulation in dNCM-PEG hydrogel

For histological evaluation, cell-laden hydrogels were fixed in 3.7% formaldehyde (Sigma-Aldrich, 11-0705) on days 0 and 14, dehydrated, and processed to wax using a tissue processor. Native porcine NP tissue was included as a positive control.

Four µm thick paraffin-embedded sections were deparaffined, rehydrated and stained with Mayer's Hematoxylin (109249, Sigma Aldrich) for 10-20 sec and Eosin solution (2.0 g/L Eosin Yellowish (Sigma Aldrich, 115935 in 50% ethanol) for 20 sec to evaluate their morphology after dehydration and mounting. Sections were imaged using a bright-field microscope (Olympus BX51; Olympus, Tokyo, Japan).

To evaluate the expression of phenotypic and ECM markers, immunohistochemical (IHC) staining for several markers (aggrecan (ACAN), brachyury (TBXT), caveolin-1 (CAV-1), collagen type II (COL II), Forkhead Box F1 (FOXF1), cytokeratin 8/18/19 (panKRT), and Paired Box 1 (PAX1); Table 2) was performed. The deparaffinized sections were blocked with 0.3% H_2O_2 for 10 min, washed with a 0.1% phosphate buffered saline (PBS)-Tween solution (PBS-T 0.1%), and antigen retrieval was performed as listed in Table 2. After washing with PBS-T solution, sections were blocked with 5% BSA in PBS for 30 min. Finally, the sections were incubated with the primary antibody (Table 2) overnight at 4 °C. The day after, the sections were washed with PBS-T solution and incubated with the appropriate secondary antibody for 30 min. The sections were incubated with the Bright-DAB substrate kit (Immunologic, VWRKBSO4-116) for 5 min after washing with PBS. After rinsing with Milli-Q® water, the sections were counterstained with Mayer's hematoxylin for 1 min. Finally, the sections were rinsed in running tap water, dehydrated, cleared, and mounted (Vectamount; H5000, Vector Laboratories, Burlingame, USA). The corresponding diluted isotype antibody was used for each antibody. Images of the sections were acquired using cellSens software (version 2.3, Tokyo, Japan) and a bright-field microscope (Olympus BX51, Tokio, Japan). To quantify the immunopositivity for the phenotypic markers, the positively stained cells were manually counted or positive area determined using Fiji plugins and divided by the total number of cells in that area. For both methods, six different areas per condition were randomly selected in images at 20 × magnification.

Table 2. Detailed information of products and protocols used for immunohistochemical stains of porcine notochordal cells and bovine nucleus pulposus tissue.

Primary antibody	Host	Conc.	Antigen retrieval	Secondary antibody	Chromogen
Aggrecan (ACAN) (Abcam, ab3778)	Mouse	11.9 µg/mL	Pronase + Hyaluronidase (60 min, 37 °C)	Brightvision poly-HRP-Anti-Mouse (Immunologic VWRKDPVM110HRP)	3,3'-Diaminobenzidine (Bright-DAB; Immunologic, BS04-110)
Brachyury (TBXT) (R&D Systems, af2085)	Goat	4 µg/mL	10 mM citrate buffer pH 6 (30 min, 70 °C)	ImmunoCruz® goat LSAB Staining System (Santa Cruz, sc-2053)	Bright-DAB
Caveolin-1 (CAV-1) (BD Biosciences, 610406)	Mouse	2.5 µg/mL	10 mM citrate buffer pH 6 (60 min, 70 °C)	Brightvision poly-HRP-Anti-Mouse	Bright-DAB
Collagen II (COL II) (DSHB, II-II6B3)	Mouse	0.375 µg/mL	Pronase + Hyaluronidase (30 min, 37 °C)	Brightvision poly-HRP-Anti-Mouse	Bright-DAB
FOXF1 (Abcam, ab168383)	Rabbit	6.9 µg/mL	10 mM citrate buffer pH 6 (30 min, 70 °C)	Brightvision poly-HRP-Anti-rabbit	Bright-DAB
Human nuclei (HuNu) (Abcam, ab190710)	Mouse	10 µg/mL	10 mM citrate buffer pH 6 (30 min, 70 °C)	Goat-anti mouse IgG, AP-conjugated (Abcam, ab97020)	StayGreen/AP (Abcam, ab156428)
Ki67 (Thermo Fisher Scientific, MA5-14520)	Rabbit	N/A	10 mM citrate buffer pH 6 (30 min, 98°C)	Brightvision poly-HRP-Anti-rabbit (Immunologic, DPVR55HRP)	Bright-DAB
Cytokeratin 8/18/19 (panKRT) (Abcam, ab41825)	Mouse	1 µg/mL	10 mM citrate buffer pH 6 (30 min, 70°C)	Brightvision poly-HRP-Anti-Mouse	Bright-DAB
mScarlet (SYST, 409 008)	Rabbit	0.67 µg/mL	10 mM citrate buffer pH 6 (30 min, 70°C)	Brightvision poly-HRP-Anti-rabbit	Bright-DAB
PAX1 (Abcam, ab203065)	Rabbit	20 µg/mL	10 mM citrate buffer pH 6 (30 min, 70°C)	Brightvision poly-HRP-Anti-rabbit	Bright-DAB

2.6 Injection of dNCM-PEG hydrogel combined with human iPSC-derived mesendoderm progenitor cells in an *ex vivo* NP model

As a next translational step, we investigated the potency of the dNCM-PEG hydrogel as a protective and instructive carrier for hMEPC injection in a bovine NP (bNP) explant culture under diurnal and dynamic loading over 28 days (Figure 1C). Bovine caudal IVDs are the most commonly used tissue source for *ex vivo* culture[38]. Bovine IVDs are comparable to healthy human discs in terms of cell type in the NP, ECM composition, geometry, diffusional distance, and biomechanical properties [14, 22, 33, 37]. In this *ex vivo* model we replicated early IVD degeneration and subjected tissue samples to

biomechanical stresses mimicking daily activities [6], and hence strived to replace the commonly used rodent models of IVD degeneration studies [37].

To prepare hMEPCs for encapsulation in the hydrogel and injection into bovine NP explants, cryopreserved cells were thawed, seeded at a density of 70,000 cells/cm^2 and cultured overnight on human rLaminin-521-coated 6-well plates in N2B27 medium supplemented with 3 µM CHIR99021, 100 ng/mL NOGGIN (Miltenyi Biotec, Leiden, The Netherlands), and 10 µM Y-27632 dihydrochloride (Tebu-bio, Heerhugowaard, The Netherlands). After 24 h of recovery, the hMEPCs were stained using the PKH26 Red Fluorescent Cell Linker Kit (Sigma Aldrich, PKH26GL) according to the manufacturer's instructions before mixing with the dNCM-PEG hydrogel.

In parallel, the effect of cryopreservation on the identity of hMEPCs was assessed by IF and compared with previously published results from Warin *et al.* 2024 [24]. Three distinct hiPSC lines from different origins were used (Life Technologies, Cat# A18944, Lot Number: 1938075; hPSCreg Name: LIMFRi001-A [43]; iPSC line published by Kilens *et al.*, 2018 [44]). These data showed maintenance of hMEPC identity after cryopreservation with > 52% ± 13% TBXT+/FOXA2+ cells (Supplementary Figure 2C, D), in consistency with previously published results for fresh MEPCs [24] facilitating potential clinical application of cryopreserved hMEPCs. Furthermore, their proliferative state was confirmed by IF staining for TBXT and Ki67 (0.25 µg/ml; Sigma Aldrich, 275R-14) showing 57% ± 19% TBXT+/Ki67+ cells (Supplementary Figure 2E, F).

2.6.1 Bovine NP explant culture under dynamic loading

NP explants (8 mm diameter, 4-6 mm height) were aseptically prepared from the first five intact proximal discs of tails from two- to three-year-old cows, obtained from a local abattoir, within 24 h of sacrifice, complying with local regulations. Different disc levels were distributed equally and randomly among the groups (day -1). Freshly harvested NP tissue (day -1) served as native and normal tissue controls (*n* = 12, 'native'; Table 3).

Hydrogel distribution after injection was visualized by injecting dNCM-PEG hydrogel stained with Procion® Red MX-5B (5% w/v; Sigma Aldrich, 404365) into normal bovine NP explants and afterwards cutting open the NP tissue in the midsagittal line. Additionally, spatial distribution was checked by adding Al_2O_3 particles to the hydrogel (10% w/v, 0.4 µm, Final Advanced Materials, Strasburg, France) and scanning with a µCT100 (Scanco Medical, Brüttisellen, Switzerland) with an energy level of 55 kVp, an intensity of 200 µA, and at a resolution of 7.4 µm.

The other bovine NP explants (*n* = 6 / group and timepoint) were cultured (10% CO_2 (pH 7.2), 5% O_2, 37 °C) in previously developed volume-controllable NP culture chambers [36, 45]. The culture medium consisted of low glucose (5.55 mM) DMEM (Gibco, 21885) with 3% FBS (F7524) and 1% P/S (Lonza 17-

602, Basel, Switzerland) mimicking hereby limited nutrients and physioxic (1-5% O_2) NP environment [5]. The medium was changed every 2-3 days by applying fresh 8 mL media per bioreactor chamber; the medium supernatant was collected with every change and stored at -20 °C until further biochemical analysis. Explants were initially equilibrated overnight to a pressure of 0.2 MPa, after which this volume was constrained to the maximum volume, *that is,* the swelling of the explants was constrained to this volume/pressure (day 0). Injections were performed through an injection port in the culture chamber with a 27G needle. This needle diameter would ideally be used in clinical practice for intradiscal injection into lumbar human discs. To induce a sGAG reduction that mimics early IVD degeneration twelve explants received a chondroitinase ABC (chABC; Sigma Aldrich, C3667) injection at a dose of 0.05 U / explant (20 µL of 2.5 U/mL reconstituted in 1% BSA in PBS) (Table 3) [36].

On day three, the degenerate explants received a second injection of 25 µL corresponding to circa 10% tissue volume with either PBS ('PBS', or dNCM-PEG hydrogel with hMEPCs encapsulated ('dNCM-PEG+hMEPCs') (Figure 1C; Table 3). The hMEPCs were formulated at a concentration of 2×10^6 cells/mL (*i.e,* 50,000 cells/explant) before injection to be on the lower side of the cell density of human native NP tissue[46] to prevent nutrient deprivation.

From day three onwards, explants were cultured with diurnal dynamic loading[6] previously shown to maintain tissue ECM composition and properties comparable to those of native samples. A static load (0.1 MPa) was applied for 6 h to mimic the inactive phase of the diurnal cycle. The active phase was mimicked by six cycles of 1 h dynamic loading (0.2 MPa – 0.4 MPa, 0.2 Hz) followed by 2 h of a static load of 0.1 MPa. A minimum of 3 hours between injection and the start of the loading cycles to achieve complete gelation of the hydrogel and gelation in a reaction tube were ensured to reduce the risk of leakage. Longitudinal biomechanical testing and metabolic monitoring were conducted, and explants were harvested on day 27 and cut into two halves in the midsagittal line: one half for biochemical analysis and one half for histological analysis.

As a control, hMEPCs encapsulated in the dNCM-PEG hydrogel were simultaneously cultured in 96-well plates until day 27 using the same cell density, culture media, and incubator settings to determine cellular survival (described below) *in vitro*. *In vitro* cell survival was investigated by imaging (Axio Observer 7, Zeiss, Germany) PKH26-labelled fluorescent hMEPCs embedded in the dNCM-PEG hydrogel in well plates. For the *ex vivo* evaluation of cell survival, one-quarter of the explants with injected cells were harvested on day 27 and imaged immediately for PKH-labelled cells. DAPI staining was performed to co-identify resident bovine NPCs.

Table 3: Overview of the experimental groups

Treatment	Dynamic loading	Injection Day 0	Injection Day 3	Harvest Day
Native	-	-	-	Day -1
PBS	+	chABC	PBS	Day 27
dNCM-PEG+hMEPCs	+	chABC	dNCM-PEG+hMEPCs	Day 27

To determine the regenerative effects of the hydrogel alone, a similar experiment was conducted in which bNP explants received an injection with either PBS or the dNCM-PEG hydrogel on day 3 and samples were collected on day 21 (Supplementary Table 2).

2.6.2 Biomechanical testing of the NP explants

A stress relaxation test was used to determine the equilibrium stress as a surrogate for intradiscal pressure during the culture period, as a change in sGAGs is correlated to the equilibrium pressure via the fixed charge density[36]. Shortly, with a mechanical testing system (MTS Criterion Model 42, MTS, MO), three preconditioning ramps of 2% compression were applied, after which a preload of 0.98 N was applied. Subsequently, a displacement of 5% was applied within 1 sec and held constant for 30 min while measuring force continuously[36]. Equilibrium stress was determined, and equilibrium pressure was calculated with the available surface area of the explants. Furthermore, height loss after 16 h of active phase and recovery after 5 h of unloading were measured in the 'PBS' and 'dNCM-PEG+hMEPCs' groups on day 25, two days before harvest.

2.6.3 Metabolic activity

To investigate the metabolic activity of the bNP explants after hMEPC injection, a glucose and lactate assay were performed on medium supernatant samples collected during the media changes over the 27-day dynamic loading culture period from the experimental group 'dNCM-PEG+hMEPCs' with the 'PBS' -group as controls as previously described [6]. This was performed to check whether cell injection would induce stress to the resident bNPCs and transplanted cells hMEPCs *e.g.* because of lactate buildup or medium consumption. Glucose concentrations were measured with an adapted colorimetric assay [47]. Briefly, a fresh buffer/chromophore reagent was prepared by mixing 3.5 mL of 10 mM 4-amino antipyrine (Sigma Aldrich, cat# 06800) with 3.5 mL of 10 mM 3-(N-ethyl-3-methylanilino) propane sulfonic acid sodium salt (Sigma Aldrich, E8506) and 3 mL of 0.8 M sodium phosphate buffer (pH 6). One hundred µL buffer/chromophore reagent was mixed with 10 µL peroxidase (1.6 U/mL; Sigma Aldrich, cat# 77332), and 10 µL glucose oxidase (2.7 U/mL; Sigma Aldrich, cat# G7141) per well and added to 2 µL sample. After 30 min of incubation at room temperature in the

dark, absorbance was measured at 550 nm, and concentration was determined with a standard curve of D-glucose from 0.08 to 10 mM. Lactate concentrations were determined by an enzymatic assay[48]. Briefly, a reaction mix was prepared to contain 5 mg/mL of β-nicotinamide adenine dinucleotide hydrate (Sigma Aldrich, N7004, 0.2 M glycine buffer (Sigma Aldrich, G5418), and 22.25 U/mL of l-lactic dehydrogenase (Sigma Aldrich, 3916). Per well, 40 µL of the sample was mixed with a 40 µL reaction mix and incubated at 37 °C for 30 min, after which absorbance was measured at 340 nm. The lactate concentration of the samples was calculated using a standard curve of sodium l-lactate (Sigma Aldrich, cat# L7022) ranging from 0.016 to 1 mM.

2.6.4 Biochemical evaluation

The halved bNP explants were weighed and frozen at -80 °C and, after lyophilization for 72 hours, weighed again to determine the relative water content. The lyophilized samples were digested overnight at 60 °C in 500 µL digestion buffer (100 mM phosphate buffer, 5 mM L-cysteine, 5 mM EDTA, and 140 µg/mL papain (Sigma Aldrich, P-5306)) [49]. dsDNA was quantified as described for the pNCs as an indication for the number of living cells. Hydroxyproline content was measured with a chloramine-T assay [50] using trans-4-hydroxyproline (Sigma Aldrich, H54409) as standard and reading absorbance at 550 nm. The collagen content was calculated by multiplying the hydroxyproline content with factor 7.5 [51]. sGAG content was quantified by 1,9-dimethyl methylene blue (DMMB) binding assay at pH 3 using chondroitin sulphate (CS) from shark cartilage (Sigma Aldrich, C4348) as standard and extracting measured absorbance at 595 nm from 540 nm. The fixed charge density (mEq/g wet tissue) was estimated by assuming a molecular weight of 502.5 g/mole and 2 moles of charge per mole of sGAG.

2.6.5 Histological evaluation

For histological evaluation, the halved bNP explants and native bovine NP tissues were fixed in 4% neutral buffered formaldehyde, processed to paraffin wax, sectioned (4 µm), and stained as described for the pNC encapsulation experiment.

To obtain an indication of the presence of proteoglycans and collagen, the bNP explant sections were stained with Alcian Blue (30 min) and Picrosirius Red (1 h) and imaged with a bright-field microscope (Axio Observer Z1, Zeiss, Germany). To assess the cell phenotype, presence of specific ECM components and cell proliferation, IHC staining was performed for several markers (ACAN, TBXT, COL II, CAV1, FOXF1, Ki67, panKRT, PAX1) using the DAB chromogen (Table 2). Furthermore, staining for Human nuclei (HuNu) was employed to allow for co-detection of the hMEPCs injected into the bNPs in the formalin-fixed deparaffinized sections for which the AP-conjugated secondary antibody was used

and visualized with the StayGreen chromogen (Table 2). Quantification of phenotypic markers with exclusive cellular expression was performed as previously described for the pNCs.

2.7 Pilot experimental *in vivo* dog study

To take the next translational step, a pilot study was performed using an experimental dog model (Figure 1D). Here we focused on investigating the medium -term survival and cell fate of the intradiscally injected hMEPCs and studied the regenerative potential of dNCM+hMEPCs on the resident disc cells. To evaluate functional differentiation of the injected hMEPCs into matrix-producing cells within the degenerate IVD host environment, the ACAN-2A-mScarlet reporter hiPSC line (TMOi001-A-14) was used as published by Tong *et al*. (2024) [52]. ACAN-2A-mScarlet reporter hiPSCs can differentiate into aggrecan-producing cells and co-express mScarlet, a marker tracing human differentiated cells that produce aggrecan. They were differentiated into hMEPCs as described in section 2.3 and directly used (*i.e.* not cryopreserved). For this study, hMEPCs were mixed with non-crosslinked dNCM as this enabled the isolation of single cells for RNA sequencing to determine the cell fate of hMEPCs and treatment effects on resident dog NPCs.

Procedures were approved and conducted in accordance with National Animal Experiments Committee guidelines (project number: AVD10800202216538) and overseen by the Local Welfare Body (working protocol number: 16538-1-01), required by Dutch regulation. One intact male Beagle (12 months of age, weight 17 kg) was purchased as a surplus animal. Four weeks before the intradiscal injections (*i.e.* T = −1 month) moderate IVD degeneration was induced in four lumbar IVDs by a board-certified veterinary surgeon via partial NP removal (NX) as previously described [17]. Shortly before T = 0, magnetic resonance imaging (MRI) was performed to determine the degree of IVD degeneration. At T = 0, four IVDs in which NX was performed were injected with 50 µL of 5×10^5 fresh hMEPCs suspended in 20 mg/mL dNCM hydrogel (L1-2; L3-4; L5-6; L7-S1). This cell number and volume was chosen taking into account the limited space and nutrient supply available in the NP. Since dNCM contains approximately half the amount of proteins as NCM [16], a double concentration of dNCM was used compared to the study conducted by Bach *et al.* 2018 [17]. At T=3 months, the dog was euthanized and the samples collected. A detailed description of the anesthesia and analgesia protocols, induction of degeneration and intradiscal injections, MRI and CT, and sample collection are provided in the supplementary Materials and Methods. The GAG, DNA, and collagen content were determined as described in section 2.6.4.

2.7.1 Single cell analysis

To assess whether the engrafted hMEPCs displayed an NC/NPC-like phenotype, and to check for off-target differentiation, together with effects on the resident dog NPCs, the L7-S1 IVD segment was collected within 3 h after termination and immediately processed. In accordance with the 3Rs principle, from an unrelated experiment we processed in parallel a non-treated IVD level of a sibling Beagle dog in which also degeneration was induced by NX at T = -1 month. Single cells from these two NPs were isolated using a two-step enzymatic digestion protocol using 3.5 U/mL pronase (11459643001, Roche) and 570 U/mL collagenase type II (LS004177, Worthington). The living single cells (detected based on the Hoechst signal) were FACS sorted into capture plates during which human cells were identified and sorted from dog NPCs with the aid of the human specific, HLA+FITC antibody (1 µg / 1 × 10^6 cells; 11-9983-42, Thermo Fisher). Capture plates with the sorted single cells were subjected to single-cell RNA sequencing at Single Cell Discoveries (Utrecht, the Netherlands) according to an adapted version of the SORT-seq protocol [53].

Bioinformatic analysis was conducted using R (R v4.4.2) using the Seurat package [54]. Based on the HLA signal the wells containing human cells were identified and removed from the dog data, whereas for the human data these wells were selected. Dog cells with total gene counts between 1,000 and 6,000, at least 500 total genes, and mitochondrial RNA <5% were retained for analysis. Human cells with total gene counts between 1,000 and 4,000, at least 500 total genes, and a mitochondrial RNA <5% percent were retained for analysis. After removing low quality barcodes, samples were normalized and integrated using the top 2000 variable genes [55]. Based on the principal component analysis (PCA), the first 9 (dog) or 5 (human) principal components (PCs) were selected for dimensionality reduction and graph-based clustering, visualized using Uniform Manifold Approximation and Projection (UMAP). Cluster marker genes were identified using Seurat's 'FindAllMarkers' (Wilcoxon rank sum test; FDR-adjusted $p < 0.05$, logFC ≥ 0.25).

2.7.2 Tracking of differentiated hMEPCs at the tissue level

Using the ACAN-2A-mScarlet reporter iPSC line [52], the presence of ACAN-producing hMEPCs was evaluated after 3 months by immunostaining for the mScarlet protein [56], besides evaluating the presence of healthy NP cell phenotypic marker TBXT (Table 2; section 2.5.2).

2.7.3 Immunogenic response

Potential systemic side-effects caused by the xenotransplantation of the hMEPCs were assessed on PBMCs isolated from blood samples at baseline, 2 weeks and 3 months post injections. PBMCs were incubated with fluorescently conjugated primary antibodies to detect phenotypic and activation markers for either T cells or monocytes (Supplementary Table 3). Furthermore, liver, lung, kidney,

testis, heart, spleen, and lymph nodes were screened for the presence of abnormalities (*i.e.* infiltration of immune cells) by a veterinary pathologist.

2.8 Statistical analysis

Statistical analysis was performed with Graph Pad Prism version 9.1.0. Normal distribution was tested by Shapiro–Wilks' test. For normally distributed data, a one- or two-way analysis of variance (ANOVA) test was used depending on the relevant number of variables and graphs show the mean ± standard deviation. The Tukey test was used to correct for multiple comparisons. When data were nonparametric, the Kruskal–Wallis test with Dunn's multiple comparison test was performed in a one-way fashion and graphs show median ± interquartile range. Statistical significance was assumed for $p < 0.05$.

3 Results

3.1 The dNCM-PEG hydrogel shows suitable injectability and rheological properties for intradiscal applications

Visibly, a cross-linked hydrogel was formed after 3 h (Figure 2A). Swelling studies were performed at different timepoints up until 96 h to observe the hydrogel behavior in media mimicking the healthy and degenerate IVD environment (Figure 2B) [5]. The hydrogel reached the maximum swelling capacity (approximately 30%) within the first 2 h without considerable weight fluctuations compared to later timepoints (Figure 2B). There were no differences found between the healthy and degenerate media, indicating that the swelling capacity of the hydrogel was not influenced by the osmolarity and pH level of the media. The dNCM-PEG hydrogel formulation mixed with hMEPCs was easily extruded through a 27 G needle before gelation, supporting the injectability for *in vivo* intradiscal application (Supplementary Video 1). The biomechanical properties, determined post-gelation of the dNCM-PEG hydrogel (*i.e*. 3 h after mixing of the hydrogel formulations), showed a storage modulus of ~ 400 Pa and loss modulus of ~ 25 Pa (Figure 2C). The properties showed a relatively soft hydrogel which is known to be favorable for NC phenotype and survival [57, 58].

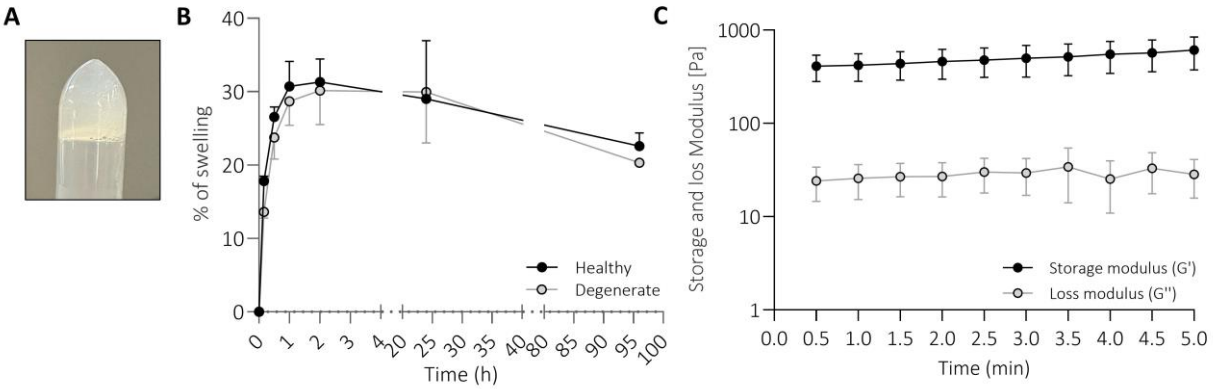

Figure 2. A dNCM-PEG-based hydrogel was fabricated with suitable rheological properties for intradiscal application. A visible hydrogel was formed 3 h after mixing the hydrogel formulations with hMEPCs (**A**). Percentage of swelling of the hydrogel in healthy (black) and degenerate (grey) disc media of the aggregated data (*n* = 3 technical replicates) (**B**). Storage modulus (G'; black) and loss modulus (G''; grey) applying shear oscillations at a constant stress of 0.5 Pa and a frequency of 1 Hz (*n* = 5 technical replicates) (**C**). Individual measurements are presented in Supplementary Figure 3.

3.2 dNCM-PEG hydrogel supports viability and NC-phenotype of porcine notochordal cells *in vitro*

To examine the ability of the dNCM-PEG hydrogel to support viability and the NC-morphology and phenotype, native pNCs were encapsulated and cultured within the dNCM-PEG hydrogel under healthy and degenerate disc conditions. pNCs were viable directly after encapsulation in the dNCM-PEG hydrogel, as indicated by the live-dead images (Figure 3A). Since the presence of NC clusters and the background signal of the hydrogel hampered proper quantification of the number of living cells during the culture period, the dsDNA content was measured as an indication of the viability (Figure 3B). On day 7, the dsDNA content showed a relative decrease (healthy 1.5; degenerate 1.3 fold change (FC)) compared to day 0, although not significant (healthy $p = 0.058$; degenerate $p = 0.400$) after which it stabilized. Thereafter, encapsulated pNCs showed stable dsDNA values throughout the culture period in both media compositions, demonstrating that the dNCM-PEG hydrogel supported NC viability under healthy or challenging degenerative NP conditions (Figure 3B).

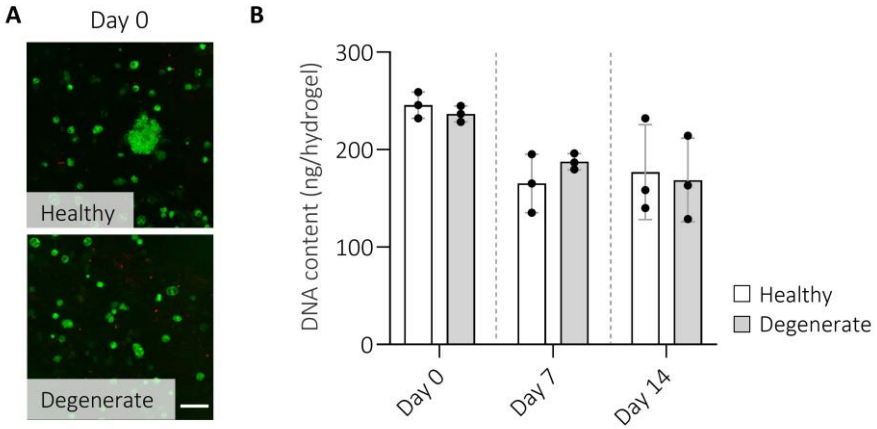

Figure 3. dNCM-PEG hydrogel supported viability of native porcine notochordal cells (pNCs). Viability of pNCs directly after encapsulated in dNCM-based hydrogel in healthy and degenerate disc medium. Scale bar = 20 µm (**A**). dsDNA content (mean ± SD) of the encapsulated pNCs on day 0, 7, and 14 in dNCM-PEG hydrogel in both media compositions. *n* = 3 technical replicates/condition prepared from 3 pooled porcine spines (Two-way ANOVA with Tukey correction; no statistical differences were observed) (**B**).

Native NCs are characterized by their cluster formation and intracellular vacuoles which are typically rapidly lost during *in vitro* cultures [22]. In line with this, we observed that the immunopositivity of several transcription factors that define the healthy NPC/NC phenotype [10] (TBXT, FOXF1, and PAX1) and the NC-phenotypic marker panKRT was diminished directly after pNC encapsulation (day 0) compared to the native tissue (Figure 4). However, the presence of vacuoles and cluster formation of pNCs was maintained as shown by H&E-stained sections and the protein expression of the vacuole marker caveolin (CAV-1) [22] (Figure 4). Remarkably, the dNCM-PEG hydrogel was able to restore the expression of NC transcription factors, as shown by increased immunopositivity for TBXT, FOXF1, and PAX1 on day 14 of culture (Figure 4) when compared to day 0. Expression of the NC phenotypic marker-set panKRT was also increasingly detected on day 14 of culture (Figure 4). Immunopositivity of all NC markers increased to comparable levels in both media conditions. Quantification showed a significant increase in TBXT (2.3 FC; $p = 0.042$), FOXF1 (5.6 FC; $p = 0.042$), PAX1 (2.2 FC; $p = 0.002$), and panKRT (202 FC; $p = 0.0027$) expression on day 14 compared to that on day 0 in the healthy medium, and only TBXT (5.2 FC; $p = 0.0007$) and CAV1 (3.3 FC; $p = 0.0042$) immunopositivity in the degenerate medium (Figure 5A-E).

To study the capacity of pNCs to produce healthy ECM, collagen type II (COL II) and aggrecan (ACAN) immunostaining was performed, demonstrating increased deposition of ACAN after 14 days compared to the starting culture point on day 0 (Figure 4). COL II was not present in the pericellular ECM on day 0 as expected after tissue digestion for cell isolation with collagenase II, whereas some cytoplasmatic staining was detected on day 14 (indicated by arrowheads in Figure 4). These results indicate that the dNCM-PEG hydrogel maintained the vacuolated phenotype and cluster formation of pNCs and

remarkably restored the expression of typical NC-phenotypic and ECM markers after 14 days of culture under normal and even degenerate disc culture conditions.

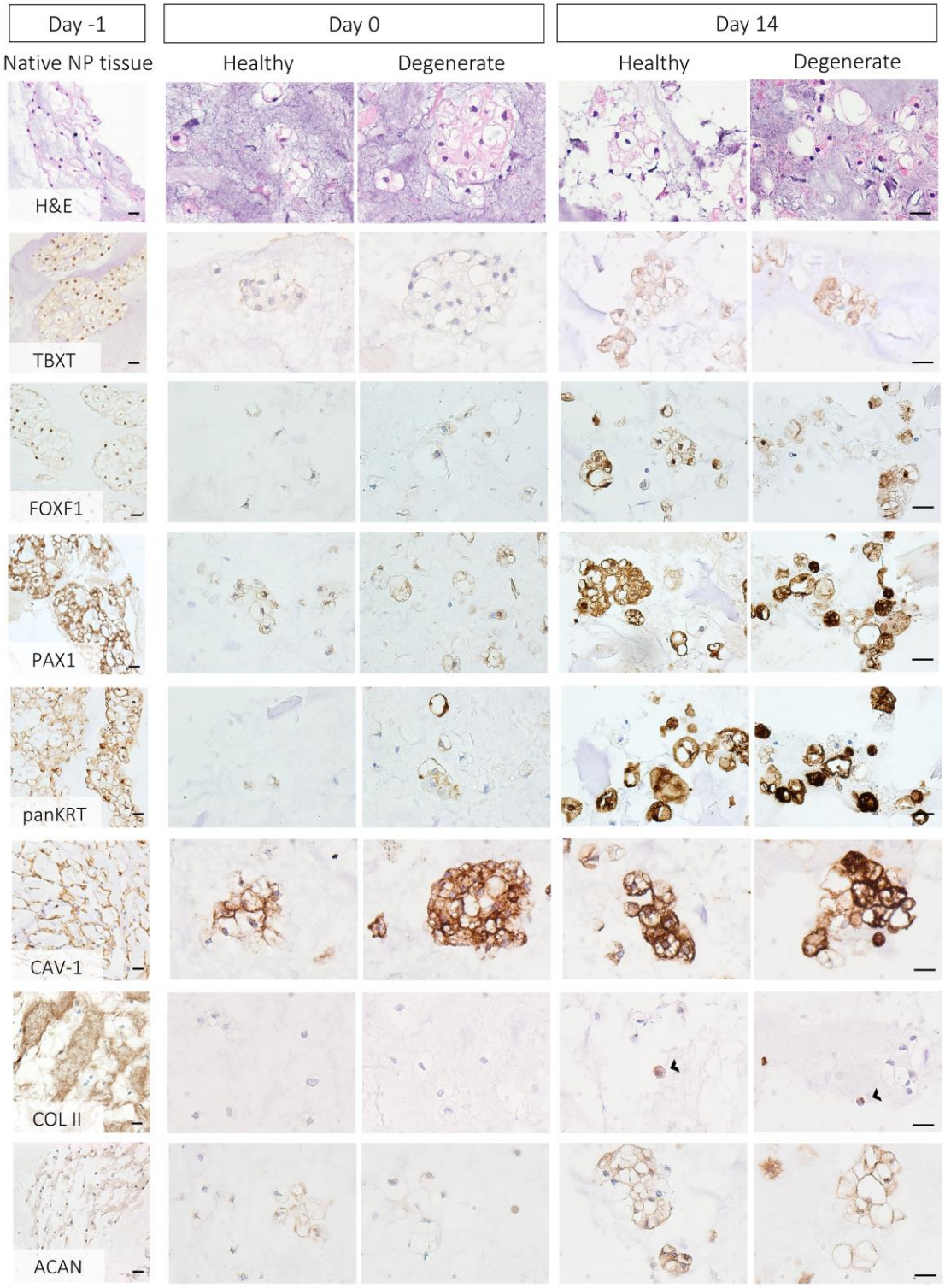

Figure 4. dNCM-PEG hydrogel maintained porcine notochordal cell (pNC) morphology and restored expression of NC phenotypic markers. Representative images of native porcine nucleus pulposus tissue and pNCs on day 0 and 14 in healthy and degenerate media encapsulated in dNCM-PEG hydrogel. Arrowheads indicate cytoplasmic COL II immunopositivity; Scale bar = 20 µm.

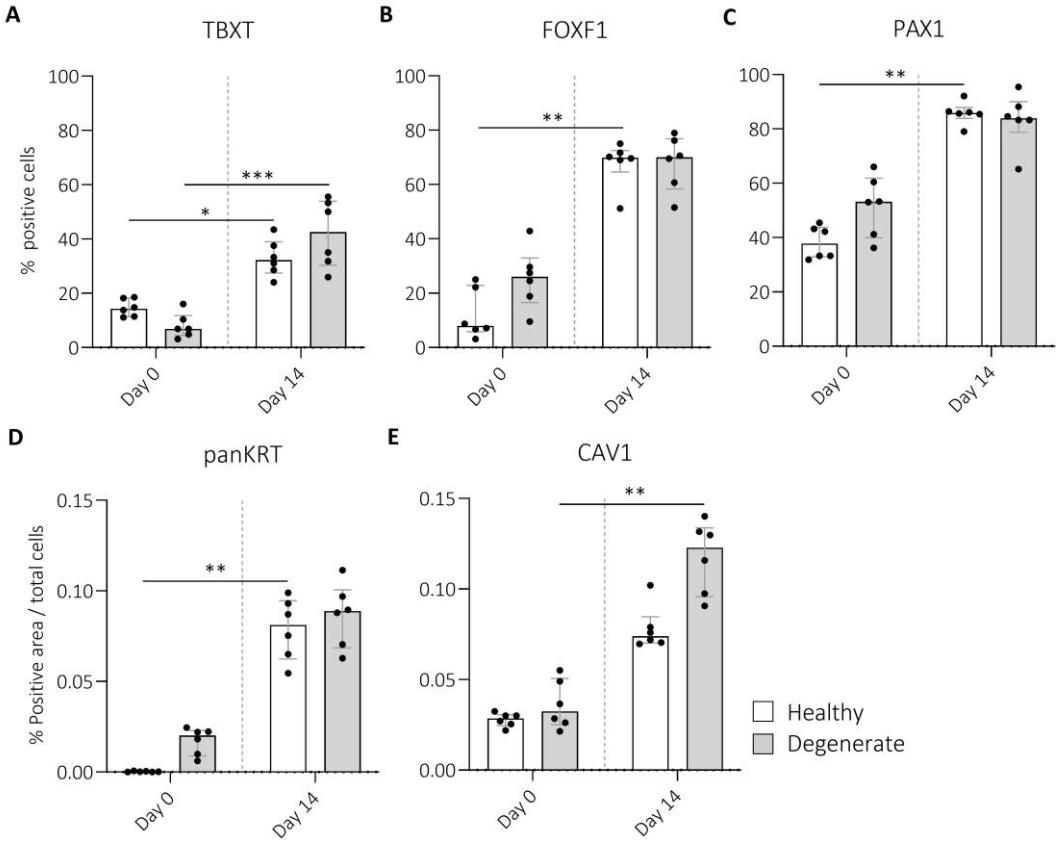

Figure 5. Expression of notochordal cell (NC)- phenotypic markers in porcine NCs is restored after 14 days of culture in dNCM-PEG hydrogel. Immunopositivity quantifications (median ± IQR) in porcine NCs cultured in healthy and degenerate disc media encapsulated in dNCM-PEG hydrogel on day 0 and 14. Graphs show % of positive cells or stained area / total cells for NC transcription factors Brachyury (TBXT) (**A**), FOXF1 (**B**), PAX1 (**C**), cytokeratin 8/18/19 (panKRT; **D**), and vacuole marker CAV-1 (**E**). *n* = 6 areas/condition. Kruskal–Wallis test with Dunn's correction; * $p < 0.05$, ** $p < 0.01$, *** $p < 0.001$.

3.3 hMEPCs guided by the dNCM-PEG hydrogel successfully engraft in the bovine nucleus pulposus explants but do not lead to biochemical restoration

The dNCM-PEG hydrogel was injected through a 27G needle (in a volume of 25 µL/explant *i.e.* approximately 10% of the NP tissue volume) and was distributed mainly in the central region of non-degenerated bNP explants, as visualized by Procion Red-colored hydrogels (Figure 6A). The central distribution in chABC-treated bNP explants was confirmed by µCT imaging (Figure 6B), and the needle tracks were visible in both the Procion Red injections and µCT images (Figure 6A,B).

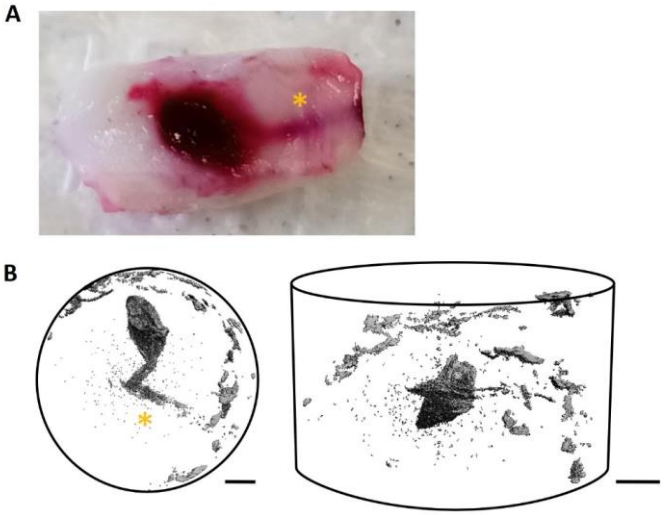

Figure 6. Distribution of dNCM-PEG hydrogel after injection into normal bovine nucleus pulposus (NP) explants. NP tissue was harvested from a bovine intervertebral disc using a biopsy punch of 8 mm diameter whereafter it was placed in the confined culture chamber. Hydrogel distribution after injection was visualized by injecting dNCM-PEG hydrogel stained with Procion Red whereafter it was dissected at the midsagittal line. In an intact bNP explant, the Procion-Red labeled hydrogel distributed centrally (**A**). Using dNCM-PEG hydrogel labeled with Al_2O_3 particles, distribution of the injected hydrogel was visualized through µCT imaging (**B**). Scale bar = 1 mm. * yellow star indicates the needle track.

Both PBS and dNCM-PEG+hMEPCs injections resulted in no observable leakage. During the injection, the operator haptically monitored the tissue back pressure, which is considered an indirect sign of an intact explant. Induction of degeneration led to decreased proteoglycan and ACAN staining in the chABC-treated bNP explants injected with PBS compared to native tissue (Figure 7A). COL II immunopositivity was unaffected, which was expected as chABC only targets the proteoglycans of the ECM. Although the bNP explants treated with dNCM-PEG+hMEPCs showed more proteoglycan staining and immunopositivity for ACAN compared to the PBS control (Figure 7A), the overall sGAG content was lower (2.3−3 FC; $p < 0.0001$) in all treatment groups compared to native samples (Figure 7B). The water content was higher (1.1 FC; $p = 0.0045$) in the PBS-treated group compared to the native samples, and this was unchanged with dNCM-PEG+hMEPCs injection (1.1 FC; $p = 0.0006$). However, it should also be noted that the native tissue was not equilibrated in the culture medium, and thus, the water content could have been lower due to tissue harvesting (Figure 7C).

Together, these changes led to a marked decrease (3.9 FC; $p < 0.0001$ for PBS and 3 FC; $p < 0.0001$ for dNCM-PEG+hMEPCs) in the fixed charge density in all treatment groups compared to that in the native tissue (Figure 7D). Both sGAG content and fixed charge density reduction were a result of the chABC injection and confirmed the successful induction of NP degeneration. The collagen content, normalized to dry weight, increased in the PBS- (1.3 FC; $p = 0.0027$) and dNCM-PEG+hMEPC-treated (1.2 FC; $p = 0.017$) groups, resulting from the change primarily in sGAG content (Figure 7B,E). In line with this, compared to day 0, the PBS and dNCM-PEG+hMEPCs groups lost approximately 50-75% of their initial

pressure after injection of chABC and culture for three days (Supplementary Figure 4A). After seven days, the equilibrium pressure was constant and did not increase over time indicating the absence of biomechanical recovery. The explant height loss compared to the original height (measured on day 0) after 16 h of loading (44% ± 5% for dNCM-PEG+hMEPCs vs. 49% ± 6% for PBS) and subsequent recovery for 5 h (5% ± 5% for dNCM-PEG+hMEPCs vs. 13% ± 11% for PBS) showed no significant differences between the groups, but suggested there was slightly less height loss in the dNCM-PEG+hMEPCs group (Supplementary Figure 4B). Together, these results indicated that there was no detectable biochemical restoration as tested at the sGAG level or at the biomechanical level within 27 days of the treatment with the dNCM-PEG hydrogel with hMEPCs.

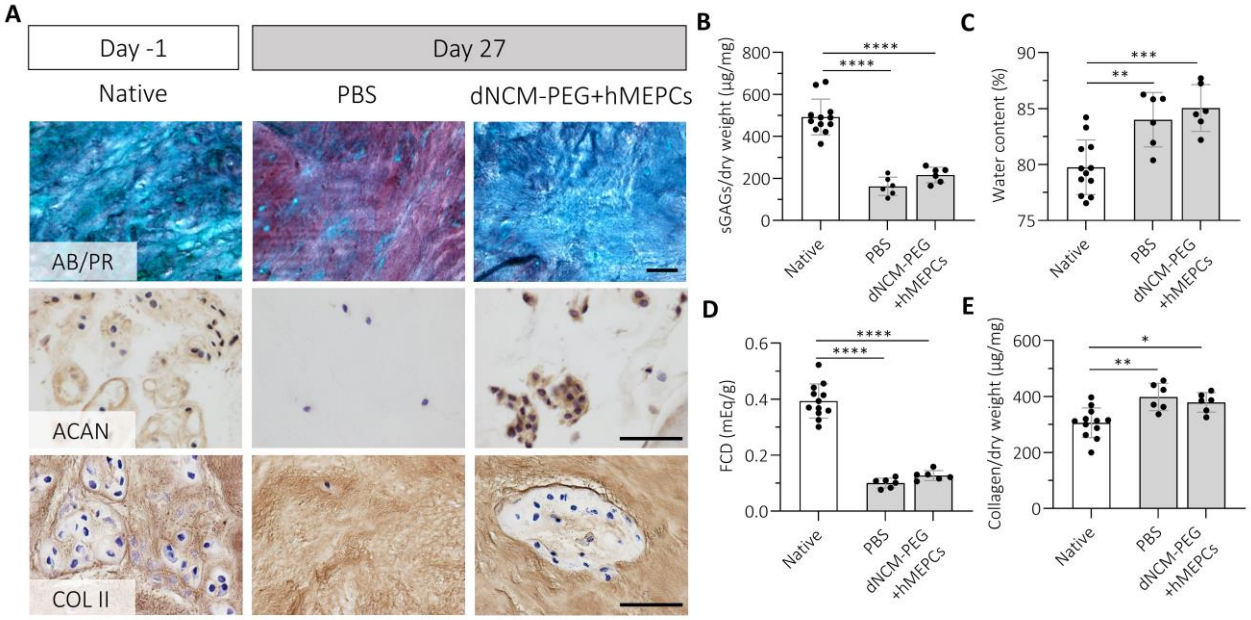

Figure 7. dNCM-PEG + hMEPC injected bNP explants show positive proteoglycan staining in contrast with PBS controls. Qualitative (**A**) and quantitative (mean ± SD; **B-E**) analysis at the tissue level of bNP explants after 27 days of culture where degeneration was induced with chondroitinase ABC. bNP explants were injected either with PBS control (PBS) or treated with 2 * 10^6 human mesendoderm cells/mL in dNCM-PEG hydrogel ('dNCM-PEG+hMEPCs'; 25 µL hydrogel delivering 50.000 hMEPCs/explant). Alcian Blue/Picrosirius Red stained sections indicated loss of GAGs in the PBS injected explants. This was confirmed by immunostainings for ACAN showing depletion of aggrecan in the extracellular matrix and cytoplasm. In bNP explants treated with dNCM-PEG+hMEPCs there was ample extracellular proteoglycan deposition, and cytoplasmic and pericellular ACAN staining on day 27. Scale bar = 50 µm (**A**). The sulphated glycosaminoglycan (sGAG) content decreased (**B**), water content increased (C), fixed charge density (FCD) reduced (**D**), and relative collagen content increased (**E**) compared to native tissue in both groups. One-way ANOVA with Tukey correction; * $p < 0.05$; ** $p < 0.01$; *** $p < 0.001$; **** $p < 0.0001$; $n \geq 6$ explants / group.

3.4 hMEPCs survive in the dNCM-PEG carrier in degenerated bovine NP explants under dynamic loading

Metabolic activity, determined by lactate release (Supplementary Figure 4C) and glucose uptake (Supplementary Figure 4D) in the medium supernatant, did not vary between the PBS- and dNCM+hMEPCs-treated groups at any time, indicating no additional metabolic stress other than the dynamic loading experienced by the cells. To further evaluate the survival of injected hMEPCs, we analyzed the PKH-26 signal and dsDNA content. These results showed that the hMEPCs cultured either in well plates or in the degenerated bNP explants remained viable for 27 days in the dNCM-PEG hydrogel (Figure 8A-C) cultured in media mimicking the disc environment under low glucose and low oxygen levels and daily loading conditions. Notably, the dsDNA content of bNP explants injected with dNCM-PEG+hMEPCs was significantly higher (2 FC; $p = 0.002$) than that of the native tissue, but not in the PBS-injected controls (Figure 8C). This finding was accompanied by immunopositivity for the proliferation marker Ki67 in dNCM-PEG+hMEPCs-treated bNP explants (Figure 8D).

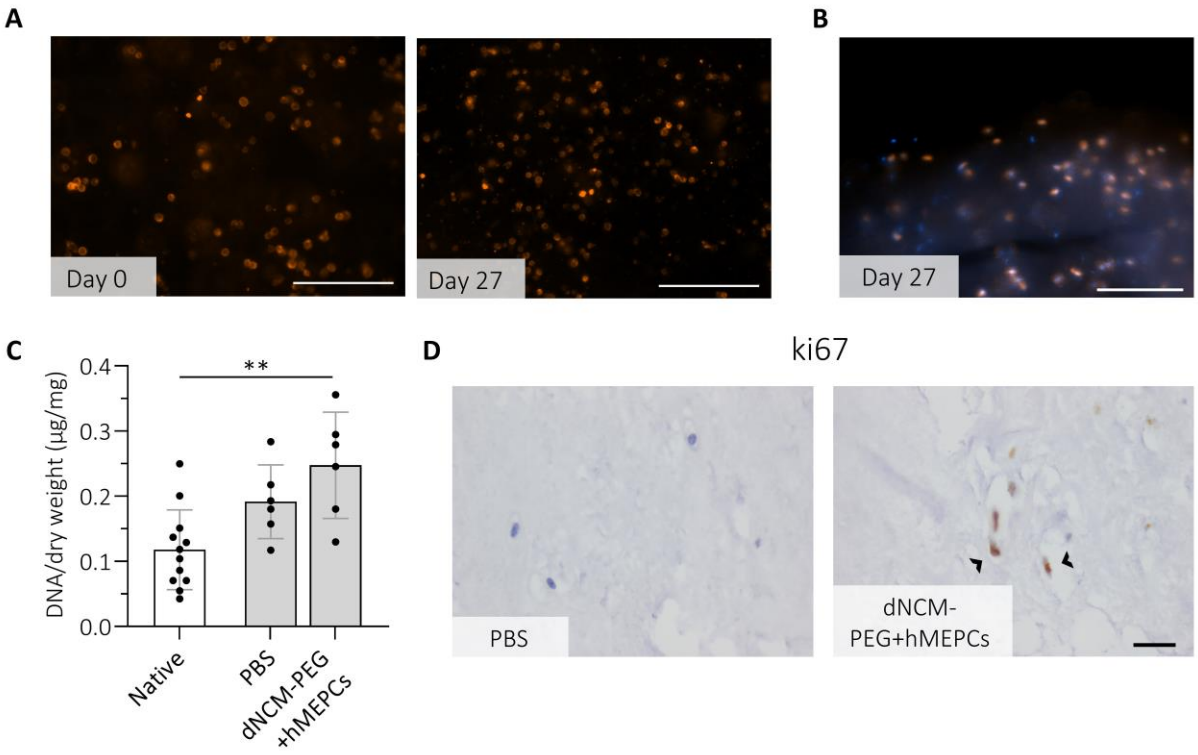

Figure 8. Human mesendoderm progenitor cells (hMEPCs) survive for 27 days *in vitro* and *ex vivo*. Fluorescently labelled hMEPCs cultured in the dNCM-PEG hydrogel were detected on day 0 and day 27 (**A**). In the nucleus pulposus explants, fluorescent hMEPCs were detected on day 27; DAPI used as nuclear counter stain showing also the presence of resident bovine NP cells (**B**). dNCM-PEG+hMEPCs injection resulted in increased DNA content (mean ± SD) compared to native NP tissue. One-way ANOVA with Tukey correction; ** $p < 0.01$; $n \geq 6$ explants / group (**C**). In line with this, proliferative cells were observed with immunohistochemical staining for Ki67, arrowheads indicate positive staining (**D**). Scale bars = 20 µm.

3.5 dNCM-PEG+hMEPCs injection improves the cell phenotype in bovine NP explants

In the native bovine NP tissue, cell clusters were present as well as expression of NC/NPC transcription factors TBXT, FOXF1, and PAX1 (Figure 9). ChABC-treatment followed by PBS injection resulted in the loss of cell clusters and decrease of the positive cells for transcription factors TBXT (79.8 FC; $p = 0.06$), FOXF1 (80.6 FC; $p = 0.012$), PAX1 (87.2 FC; $p = 0.0083$), and CAV1 (51.3 FC; $p = 0.18$) compared to control native tissue confirming successful induction of degeneration (Figure 9). In bNP explants injected with dNCM-PEG+hMEPCs, cell clusters were present and increased immunopositivity for the transcription factors TBXT (93.8 FC; $p = 0.0008$), FOXF1 (11.1 FC; $p = 0.0045$), PAX1 (8.1 FC; $p = 0.0118$), panKRT (58.7 FC; p = 0.0015), and CAV1 (83.6; $p = 0.0037$) compared to PBS-treated NP explants (Figure 9). PKH-26 labeling was undetectable due to processing of the tissue sections, which did not allow for direct detection of the PKH-labeled hMEPCs. To determine the origin of TBXT-expressing cells, co-detection with the human nucleoli marker (HuNu) was conducted, which exclusively stains cells of human origin. TBXT expression was observed in cells that also showed immunopositivity for HuNu confirming the engraftment of hMEPCs as well as in HuNu-negative cells, the latter indicating the expression of TBXT in resident bovine NPCs (Figure 9).

Consistent with these beneficial effects of dNCM-PEG+hMEPCs by resident cells and tissues, we conducted a follow-up study to investigate the performance of the hydrogel alone at 21 days (Supplementary Table 2). Similar to the previous experiment, NP degeneration was successfully induced, as evidenced by Alcian Blue/Picrosirius Red staining, which showed decreased proteoglycan staining in PBS-treated bNP explants compared to native bNP explants (Supplementary Figure 5A). This reduction was less pronounced after injection of the dNCM-PEG hydrogel, as confirmed by the immunopositivity for ACAN (Supplementary Figure 5A). Compared to the native bNP tissue, the water content was significantly increased (1.1 FC; $p = 0.0036$, Supplementary Figure 5B), and the sGAG content was significantly reduced (2.1 FC; $p < 0.0001$, Supplementary Figure 5C), resulting in considerably decreased fixed charge density (2.8 FC; $p < 0.0001$, Supplementary Figure 5D) for dNCM-PEG-treated groups. dNCM-PEG treatment significantly increased collagen content compared to native NP tissue (1.4 FC; $p = 0.0003$, Supplementary Figure 5E), while there was no significant change in DNA content (Supplementary Figure 5F; $p = 0.087$). These results together indicate that, comparable to the results seen with the dNCM-PEG+hMEPCs injection, there was no biomechanical restoration within 21 days of treatment with the dNCM-PEG hydrogel alone (Supplementary Figure 5G). Nonetheless, at the tissue level, extracellular and cytoplasmic ACAN and COL II immunopositivity was consistently observed in the dNCM-PEG-treated bNP explants compared to PBS, where it was largely absent (Supplementary Figure 5A). Furthermore, dNCM-PEG injection was accompanied by immunopositivity

of TBXT, FOXF1, PAX1, panKRT, and CAV1 at 21 days of follow-up, comparable to treatment with dNCM-PEG+hMEPCs (Supplementary Figure 6).

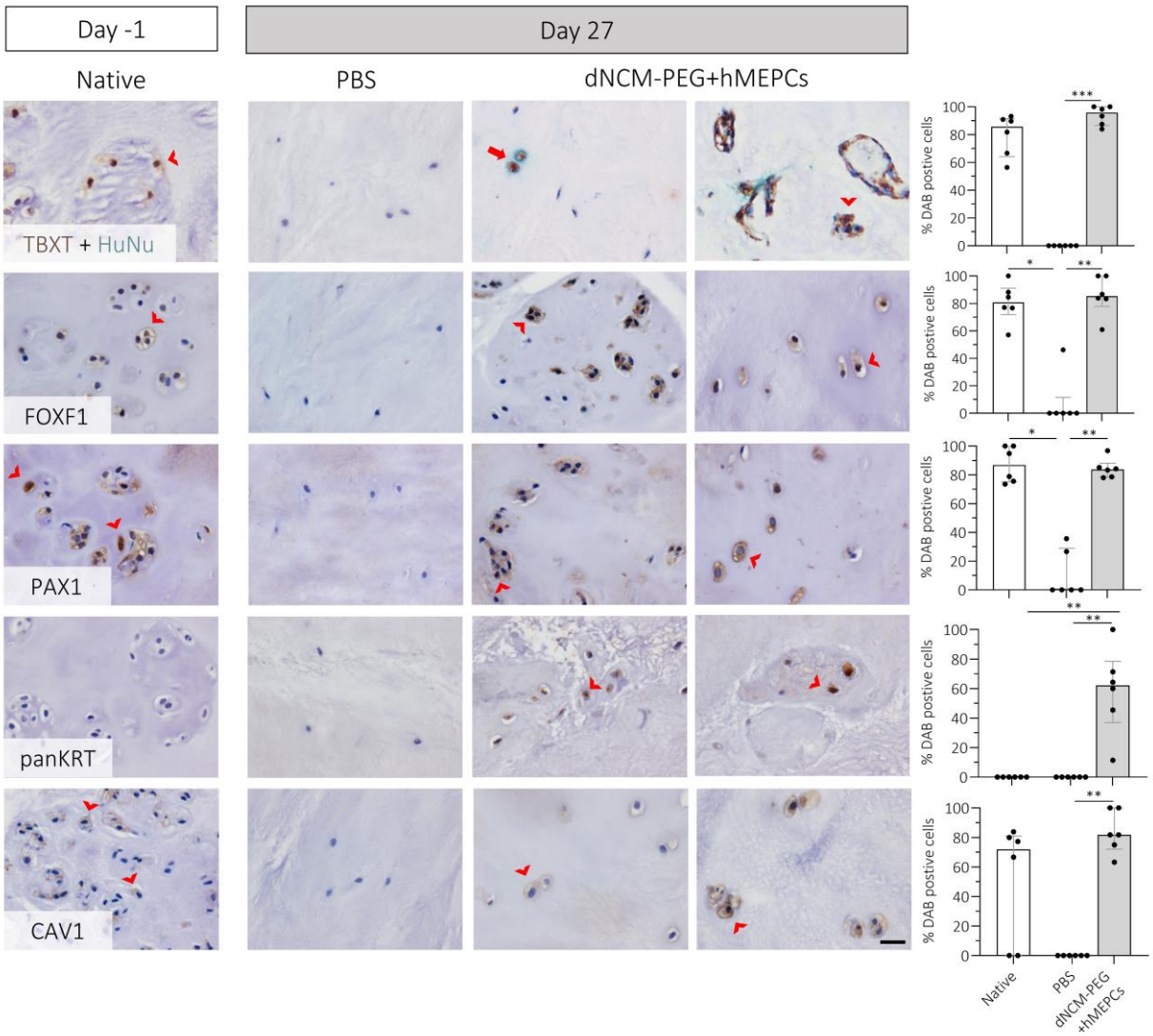

Figure 9. dNCM-PEG+hMEPC injection results in improved phenotype in bovine NP explants. Images show immunohistochemical staining for Brachyury (TBXT), FOXF1, PAX1, cytokeratin 8/18/19 (panKRT), and Caveolin 1 (CAV1) in brown using the DAB chromogen. Immunohistochemical staining for human nucleoli (HuNu) is stained green using the StayGreen chromogen to demonstrate the presence of engrafted human MEPCs. Arrowheads indicate positive DAB staining and arrow indicates double positive staining for DAB and StayGreen (scale bar = 20 µm). Quantification of DAB immunopositivity is shown in % of positive cells / total cells (median ± IQR) for TBXT, FOXF1, PAX1, panKRT, and CAV1. Kruskal–Wallis test with Dunn's correction; * $p < 0.05$, ** $p < 0.01$, *** $p < 0.001$.

These results indicate that the hydrogel alone also exerted beneficial effects on the resident bNPCs and tissue. However, the significant increase in dsDNA content was exclusively observed when the hMEPCs were added (Figure 8C, Supplementary Figure 5F).

3.6 Intradiscally injected hMEPCs guided by dNCM successfully engraft showing combined treatment exerts tissue anabolic effects in a dog disc degeneration model

To further explore the potency of hMEPCs supported by dNCM, we performed a pilot study using a validated preclinical dog model [15, 59]. Initially, moderate degeneration was induced by partial nuclectomy (NX) in alternate IVD levels. One month after induction, these levels were intradiscally injected with dNCM+hMEPCs on T=0 (Figure 10A). Three months after the treatment, the IVDs were harvested. Three injected (L1-2, L3-4, L5-6) and native discs (T13-L1, L2-3, L4-5) were used for biochemical and histological analysis (Figure 10A; indicated in black) and the L7-S1 level was processed for single cell RNA sequencing. A disc (T12-13) in which NX was performed of a dog of the same litter that was not treated with dNCM+hMEPCs was used as degenerated control (Figure 10A; indicated in grey).

Analysis of T2 weighted-MRI images demonstrated a median Pfirrmann score of 2.3 (range 2.3-3) in noNX IVDs and a median of 3 (range 2.7-3) in NX IVDs at T = 0 (4 weeks after NX; Supplementary Figure 7) confirming the degeneration model. Three months after intradiscal injections, the dNCM+hMEPCs injected IVD stabilized with median score of 3 (range 2.7-3.3) (Supplementary Figure 7), whereas the range of controls for untreated NX discs after 3 months follow-up increased to 3-4 in previous experiments[60]. Biochemical analysis demonstrated that dNCM+hMEPCs injections significantly increased the DNA and GAG content of the NP compared to the native lumbar discs of the same dog, whereas the slight increase in collagen content was not significant (Figure 10B-D).

FACS results of the enzymatically digested NP tissue showed 5.6% of cells in the disc injected with dNCM+hMEPCs were HLA^+ indicating engraftment of the hMEPCs after 3 months follow-up (Figure 10E). Relating this to the 5×10^5 injected hMEPCs, this would indicate that approximately 6.7% of the injected hMEPCs engrafted in the NP tissue. This estimate is based on the 6×10^5 cells isolated from the injected disc following tissue digestion and may represent a slight underestimation, as not all NP cells may have been recovered during the process.

After filtering, the engrafted hMEPCs dataset consisted of 233 cells and 6710 genes. Interpretation of the filtered data requires caution: despite expected library sizes and high percentages of mapped reads, the total UMI were low indicating the presence of low-quality cells. These cells were removed with the quality filters resulting in lower cell numbers with acceptable quality. Cluster-analysis showed 3 different clusters (*n* = 133, 66, and 34 cells; Supplementary Figure 8A), with cluster 1 displaying differentially expressed genes (DEG) of inflammatory cytokine genes (*TNF, IL1B*), and a gene (*FN1*) associated with inflammation and fibrosis [61] as well as the NC matrisome [24, 62, 63]

(Supplementary Figure 8B; Supplementary Table 4). The DEGs were insufficient to support precise lineage annotation.

To evaluate the lineage commitment of the engrafted hMEPCs, we conducted a supervised single-cell analysis without taking clusters into account and using different gene panels as previously published by Warin *et al.* (2024) [24] (Supplementary Table 4): only *Sex-determining Region Y-Box* (*SOX)9* expression was detected in 16% of the cells (Supplementary Figure 8C). None of the common healthy NP markers (*e.g., TBXT, KRT8/18/19*; Supplementary Table 6) were expressed by the engrafted hMEPCs except for *CAV1*, which was expressed by 3.9% of the cells (data not shown). To further explore the functional ECM-producing capacity of the engrafted hMEPCs, the data were checked for the presence of ECM anabolic and catabolic/inflammatory genes [24, 52, 64-66]. Interestingly, *ACAN* and *Collagen* (*COL)2A1* were expressed by 50 and 58% of the engrafted hMEPCs, respectively, with 34% co-expressing these two main ECM components of the healthy NP (Figure 10F; Supplementary Figure 10A,B). Using the ACAN-2A-mScarlet reporter iPSC-line[52] the presence of ACAN-producing engrafted hMEPCs was further supported by immunopositivity (~2.5% of the cells) for the mScarlet protein in the treated IVDs (Figure 10G). Additionally, other NC- associated matrisome markers were expressed *e.g. Secreted Phosphoprotein 1 (SPP1)*, *Fibronectine-1 (FN1)*, *Galactin-3 (LGALS3)* [24, 62, 63] (56%, 95%, 99% respectively) as well as proteoglycans *Syndecan-4 (SDC4), Versican (VCAN)*, and *Decorin (DCN)* (92%, 45%, 33%, respectively) (Supplementary Figure 9). Further analysis revealed that cells expressing catabolic/inflammatory markers did not segregate based on the expression of $ACAN^{+}/COL2A1^{+}$ or the absence thereof $ACAN^{-}/COL2A1^{-}$ (Supplementary Figure 10B,C). Hence, hMEPCs expressing catabolic/inflammatory markers did not represent a dysfunctional cell population.

After filtering, the resident dog single cell NPC population consisted of 515 cells and 11,170 genes, which could be distributed in three distinct clusters (Figure 10H). Most cells derived from the degenerated NP control appeared in cluster 0 (n = 226 cells), whereas cells derived from the dNCM+MEPC-treated NP were in cluster 1 and 2 (n = 262; n = 27 cells, respectively) (Figure 10H). Such clear variations in their cluster distribution indicate a different expression profile between treated and untreated IVDs. Within the top 20 DEGs, inflammatory and degenerative markers [67-69] *Periostin* (*POSTN), High Temperature Requirement A Serine Peptidase 1 (HTRA1),* and *COL18A1* while cluster 1 was characterized by increased expression of protective marker [70] *Chitinase-3-Like Protein 1* (*CHI3L1*) and proteoglycan *VCAN* (Supplementary Figure 11). Supervised analysis using selected marker sets to distinguish between the NPC and NC phenotype (Supplementary Table 6 [71]), showed comparable expression levels of NC-marker *Thy-1 Cell Surface Antigen (THY1)* in cluster 0 and 1, whereas cluster 2 showed almost no expression (Supplementary Figure 11B). NPC-marker *Proteoglycan 4 (PRG4)* was present in all clusters with a comparable expression profile, whereas

RUNX1 expression was low in all clusters (Supplementary Figure 11B). Other phenotypic markers found in the healthy NP (*KRT8, KRT18, KRT19, CAV1, PAX1, FOXF1*; Supplementary Table 6) were also not differentially expressed between the clusters. Focusing on ECM anabolic and catabolic markers[64, 72-74] (Supplementary Table 5), cluster 1 showed a higher expression of *VCAN, COL2A1, COL3A1, COL9A1, COL9A3* compared to cluster 0, whereas the latter showed higher expression of aforementioned catabolic markers (*POSTN, HTRA1,* and *COL18A1*) (Figure 10I). There was no differential expression of angio-neurogenesis associated genes clusters. Cluster 2 was characterized by lower expression of most proteoglycans and collagens compared to cluster 0 and 1 except for *SDC4* and *COL1A2* (Figure 10I). Notably, this cluster showed the highest expression of most catabolic/inflammatory markers *e.g. C-C Motif Chemokine Ligand (CCL)3*, *CCL4*, *CCL5*, *C-X-C Motif Chemokine Ligand (CXCL)10*, *Interleukin 1 Beta (IL1B)*, *Matrix Metallopeptidase (MMP)9*, *Signal Transducer and Activator of Transcription (STAT)1*, *STAT3*, which together with the loss of NC/NPC phenotypic markers, indicates the dog NPCs in this cluster had a more catabolic/inflammatory phenotype.

Gene expression of key NC marker TBXT was not detected in the single cell data set. In light of the technical limitations encountered resulting into low UMIs, we extended the analysis at the protein level. TBXT immunopositivity was detected in ~5% of the cells in the dNCM+hMEPC-treated NPs (Figure 10G) whereas only one single positive cell was detected (L6-L7) across all three native IVD levels (Supplementary Figure 11C). To further investigate the working potential mechanisms underlying dNCM+hMEPCs-induced regeneration, we analyzed key pathways in the single cell data (Supplementary Table 7) [75], but probably limited by the low cell numbers and limited complexity of RNA features, found no distinct transcriptomic differences in pathway regulation between the injected and degenerate control disc (Supplementary Figure 11D).

Flow cytometry analysis of the isolated PBMCs demonstrated slight activation of T-cells and monocytes indicated by increased $CD3^+/CD69^+$ and $CD14^+/CD86^+$, respectively (Supplementary Figure 12A-B) at T = 6 weeks compared to baseline samples. However, normalization at T = 3 months indicated no relevant immunogenic response to the injected treatment. There were no abnormalities on the CT-scans (*e.g.* extra-discal mineralization or other bone abnormalities) or on macroscopic and microscopic level of the collected organs (liver, lung, kidney, testis, heart, spleen, and lymph nodes), nor was there cell infiltration observed in the three dNCM+hMEPC-treated discs (H&E-stained sections; Supplementary Figure 12C). As an additional assessment of teratoma risk, the expression of pluripotency markers (*Alkaline Phosphatase (ALPL), LINE-1 Type Transposase Domain Containing 1 (L1TD1), SOX2, Octamer-binding Transcription Factor 4 (OCT4)*) was evaluated in the hMEPC sorted cells and found to be absent. However, due to low sequencing depth, definitive conclusions regarding undetected genes cannot be drawn.

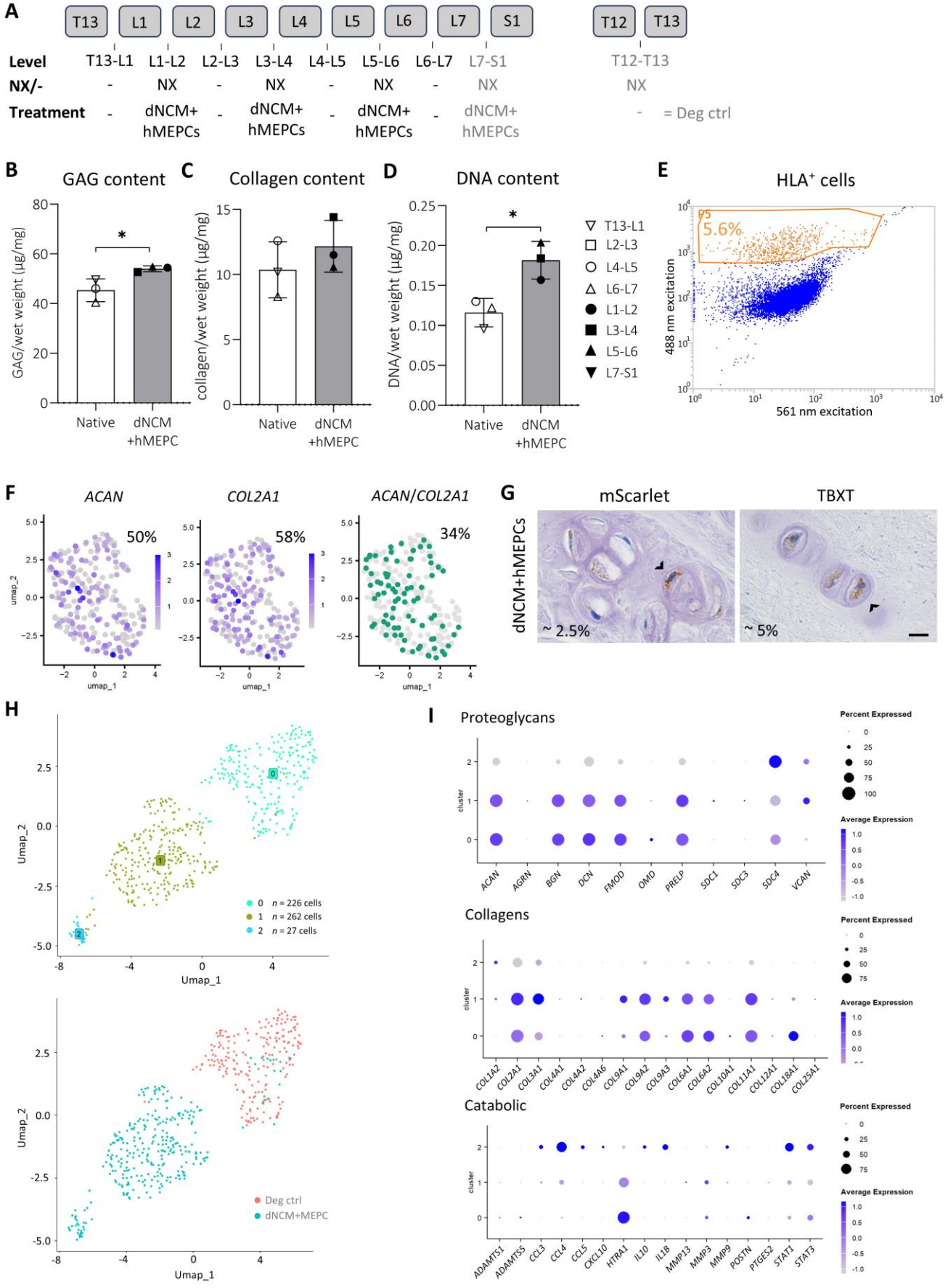
A
T13
L1
L2
L3
L4
L5
L6
L7
S1
T12
T13
Level
T13-L1
L1-L2
L2-L3
L3-L4
L4-L5
L5-L6
L6-L7
L7-S1
T12-T13
NX/-
NX
Treatment
dNCM+ hMEPCs
= Deg ctrl
B
GAG content
GAG/wet weight (µg/mg)
Native
dNCM +hMEPC
C
Collagen content
collagen/wet weight (µg/mg)
D
DNA content
DNA/wet weight (µg/mg)
T13-L1
L2-L3
L4-L5
L6-L7
L1-L2
L3-L4
L5-L6
L7-S1
E
HLA+ cells
5.6%
488 nm excitation
561 nm excitation
F
ACAN
COL2A1
ACAN/COL2A1
50%
58%
34%
umap_1
umap_2
G
mScarlet
TBXT
dNCM+hMEPCs
~ 2.5%
~ 5%
H
Umap_1
Umap_2
0 n = 226 cells
1 n = 262 cells
2 n = 27 cells
Deg ctrl
dNCM+MEPC
I
Proteoglycans
ACAN
AGRN
BGN
DCN
FMOD
OMD
PRELP
SDC1
SDC3
SDC4
VCAN
Collagens
COL1A2
COL2A1
COL3A1
COL4A1
COL4A2
COL4A6
COL9A1
COL9A2
COL9A3
COL6A1
COL6A2
COL10A1
COL11A1
COL12A1
COL18A1
COL25A1
Catabolic
ADAMTS1
ADAMTS5
CCL3
CCL4
CCL5
CXCL10
HTRA1
IL10
IL1B
MMP13
MMP3
MMP9
POSTN
PTGES2
STAT1
STAT3
Percent Expressed
Average Expression
cluster

Figure 10: Human MEPCs guided by dNCM survive and obtain a functional matrix-producing phenotype after 3 month follow-up in a preclinical dog model with a small proportion obtaining a degenerative phenotype. Graphical representation of the treatment conditions with treatment injected 1 month after partial nuclectomy (NX). hMEPCs were mixed with non-crosslinked dNCM as this enabled the isolation of single cells for RNA sequencing to determine the cell fate of hMEPCs and treatment effects on resident dog NPCs. A disc (T12-T13) of a dog from the same litter used in an unrelated animal experiment served as degenerate control (Deg ctrl) for the single cell analysis (**A**). Biochemical analysis of the nucleus pulposus (mean ± SD; One-way ANOVA with Tukey correction; * $p < 0.05$;) (**B**-**D**). HLA-labelled cells of the enzymatically digested L7-S1 segment subjected to flow cytometry and single cell sorting for single cell RNA-seq (**E**). UMAPs indicating *COL2A1, ACAN*, and *COL2A1/ACAN* double (indicated by green dots) positive cells within the hMEPC population (**F**). Immunostains for mScarlet and TBXT in dNCM+hMEPC injected NPs with arrowheads indicating positive cells per NP tissue section (scale bar = 20 µm) (**G**). UMAPs of the dog cells showing cluster separation and cell origin (**H**). Dot plots showing expression of proteoglycan, collagen, and catabolic genes within the different dog cell clusters (**I**).

4 Discussion

In this study, we successfully integrated the widely recognized regenerative potential of NCs into a user-friendly hydrogel that builds upon the widespread use of natural biomatrices and their capacity to replicate the tissue-specific environment. This approach resulted in a nature-inspired bioactive hydrogel that supported regenerative processes and serves as an instructive cell carrier providing the necessary cues for injected cells to survive, engraft, and thrive in the harsh IVD environment. This instructive cell carrier achieved maintenance, even under degenerative disc culture conditions, of the phenotype of native NCs, which are well-known for the difficulty in maintaining their vacuolated phenotype in culture. Furthermore, this work showed the translational potential of NC-based therapies combined with a bioactive material containing part of the NC secretome in the form of dNCM in a clinically relevant advanced *ex vivo* culture system mimicking the degenerate IVD during daily life loading. Preliminary data demonstrate that the hMEPCs successfully engrafted and obtained a functional ECM-producing phenotype after intradiscal injection together with dNCM in a preclinical dog model. This combined treatment resulted in tissue anabolic effects after 3 months follow-up with a small sub-population of resident NP cells presenting with a catabolic/inflammatory phenotype.

4.1 dNCM-PEG hydrogel shows suitable properties for a cell-based intradiscal application

The dNCM-PEG hydrogel formulation, containing 15 mg/mL dNCM cross-linked with 8-arm PEG was easily extruded through 27 G before gelation and showed a swelling capacity comparable to other HA-based hydrogels [76]. Even though there was a fast initiation of gelation (within 30 s), an incubation time of 3 h at 37 °C was required to achieve full gelation. We hypothesize that as more amine and carboxyl groups are used, fewer remain available, tapering the kinetics of the reaction. In a clinical application the hydrogel would be mixed with the cell product and thereafter injected intradiscally under fluoroscopic guidance. Under such conditions, a longer gelation time during which the hydrogel remains injectable is preferred and could even enhance cross-linking between the hydrogel and/or its

components, and the native tissue, facilitating bio-integration, as previously shown by an HA-hydrogel cross-linked with PEG [77]. However, more studies are necessary to determine the exact gelation behavior of the dNCM-PEG hydrogel inside the disc and its ability to integrate via crosslinks within the native ECM. Furthermore, Procion Red-stained dNCM-PEG hydrogel injections into bNPs were distributed within the tissue, filling fissures of the explants, while remaining in explants where exterior fissures were absent. It is therefore imperative to highlight that such intradiscal approaches can be applied in IVDs, where the annulus fibrosus and endplates are intact and the limited injection volume for the NP is respected [36]. The low storage modulus (400 Pa) of dNCM-PEG did not immediately restore the swelling behavior of the degenerated bNP explants, but a low storage modulus could contribute to restoration of the pig NC phenotype and to guiding the hMEPCs in the hydrogel to the NC lineage, as previous studies have reported that softer substrate stiffness are essential for the NC-phenotype [31, 78]. This also aligns with the softer biomechanical environment found in IVDs rich in NCs than that found in IVDs rich in NPCs [33-35].

4.2 dNCM-PEG hydrogel protects the typical morphology of native NCs and restores their phenotype

The dNCM-PEG hydrogel supported the maintenance of cell clusters and CAV-1^{+}-vacuoles of porcine primary NCs in both healthy and degenerate disc-mimicking media. Furthermore, it restored their phenotype marked by the presence of NC- and healthy ECM markers. This is a promising finding, since most studies report that the NC-specific phenotype is already lost during extraction [79] and is very challenging to restore ormaintain using monolayer [80-83] as well as 3D-culture systems [84]. Previous *in vitro* studies only demonstrated retention of vacuolated cells expressing NC markers under very specific, non-degenerate, culture conditions [22, 85, 86]. This is the first study to demonstrate the presence of vacuoles and NC-marker expression after 14 days of *in vitro* culture in a medium that mimics the degenerative state of the NP. This implies that the dNCM-PEG hydrogel provides the necessary protective and instructive microenvironment for the NCs to restore their characteristic phenotype and matrix production, even when subjected to harsh degenerated IVD medium.

4.3 dNCM-PEG hydrogel serves as instructive cell carrier and induces a healthy cell phenotype

The cryopreserved injected human iPSC-derived MEPCs, together with dNCM-PEG as a carrier, engrafted and thrived in the degenerate bovine NP explants as indicated by the PKH26 red fluorescent signal and co-expression of HuNu and TBXT. Furthermore, higher cellularity was observed in explants that received dNCM-PEG+hMEPCs injections, but not in dNCM-PEG-alone treated explants, characterized by cell clusters and Ki67 immunopositivity indicative of increased cell proliferation. This

849 could be due to the proliferative effect on the resident bovine NPCs, in line with previous reports [16,
850 18, 36], as well as the proliferation of the injected hMEPCs.

851 Injection of the dNCM-PEG hydrogel with and without hMEPCs restored the expression of healthy
852 NPC/NC phenotypic markers (TBXT, FOXF1, PAX1, CAV1, and panKRT) and the most important ECM
853 component, aggrecan, in bNP explants cultured in low glucose, tissue physiological conditions, and
854 subjected to a loading regime mimicking daily activities. In line with this, dNCM-PEG with and without
855 hMEPCs injection also increased the Alcian Blue staining intensity of tissue sections compared to the
856 PBS group, which together could indicate partial proteoglycan restoration of the degenerate NP tissue
857 due to the hydrogel injection. Although not confirmed at the explant level by sGAG content
858 quantification, the immunostaining indicated that specifically aggrecan is enriched in the pericellular
859 matrix of treated explants. As aggrecan is a core protein for GAG attachment, its presence on
860 immunostaining may indicate early aggrecan expression before GAG decoration. This conclusion is
861 drawn within a relevant context, that is, the low metabolic rates of NPCs within the disc environment
862 and the time needed to recover the proteoglycan content by cell production alone are estimated to be
863 several months [46]. Several other factors affect the rate of GAG production, including the cell
864 phenotype and number of transplanted and resident cells. NCs have 2−4-fold higher GAG production
865 and higher metabolic activity than bovine NPCs [13, 14]. Hence, the rate of proteoglycan synthesis also
866 depends on the differentiation efficiency of hMEPCs toward matrix-producing cells, the stimulation of
867 resident cells to produce matrix, and the number and metabolic activity of the injected cells. Per
868 explant 0.5×10^5 cells were injected with an estimated tissue volume of 0.3 cm^3. This could be
869 considered a low number considering that the cell density in the native normal bovine NP is estimated
870 to be approximately $3–6 \times 10^5$ cells/0.3 cm^3 (per explant) [40]. Nevertheless, a relatively low cell
871 number for injection has two main advantages over higher cell numbers. First, there is a better chance
872 of cell survival of both injected and resident cells and for the cells to fulfill their therapeutic tasks, as
873 with increasing cell density, the nutrient demand and waste accumulation increases [4]. The
874 unaffected lactate and glucose content in the medium suggest that the cell density used in the present
875 study did not cause nutrient deprivation and waste accumulation (lactate) which could lower the pH
876 and thereby cause additional stress to the transplanted hMEPCs and resident NP cells. Follow-up
877 studies should determine the optimal cell density that results in the highest therapeutic effect without
878 overpopulating the NP.

4.4 Intradiscally injected hMEPCs engraft and obtain a functional phenotype in a dog disc degeneration model

To take the next translation step, hMEPCs were intradiscally injected together with non-crosslinked dNCM in a preclinical dog model. To date, iPS-NLCs and iPS-NP cells have been generated using (a mix of) specific medium supplements (*e.g.* TGF-β_3, GDF-5, BMP-4, and FGF), with varying degrees of success [25-28]. As opposed to this approach, in this work, we co-injected hMEPCs with dNCM with the aim to provide a tissue-specific cocktail of natural cues to direct them further to the NC-lineage. Recently it was shown that differentiation of disc-derived hiPSCs using dNCM resulted in an increased expression of healthy phenotypic and matrisome-related NP markers compared to the use of only TGF-β [87]. The present study, using blood-derived fresh hMEPCs, demonstrated that part of the injected hMEPCs engrafted after 3 months follow-up. Furthermore, a subset of the engrafted hMEPCs acquired a functional phenotype characterized by protein expression of mScarlet, indicative of differentiated hMEPC into an ACAN producing phenotype and further substantiated at the transcriptomic level by the co-expression of anabolic markers/healthy matrix markers *ACAN* and *COL2A1* and expression of other proteoglycans involved in tissue homeostasis [88], *VCAN* and *DCN*. Additionally, other markers linked to the NC matrisome [24, 62, 63] (*SPP1, FN1, LGALS3*) were expressed by at least half of the engrafted hMEPC population. However, co-expression of catabolic and inflammatory markers suggests a multifaceted phenotype that requires further studies at single cell resolution to understand lineage commitment within the disc environment. Definitive differentiation into an NC-like identity could not be confirmed by the single cell RNA sequencing data. The expression of *ACAN* and *COL2A1* indicate differentiation to matrix-producing cells imperative for a regenerative response, however other marker genes were not consistently identified.

Regenerative effects of the injected dNCM+hMEPCs were observed at the matrisome level in the resident dog NP cells. The majority of the resident dog NPCs displayed an anabolic response [70, 88, 89] to the dNCM+hMEPC treatment marked by increased expression of *VCAN, COL9A1, CHI3L1* and decreased expression of degenerative/catabolic markers [67, 68] *COL18A1, POSTN* compared with the degenerate control. Notably, a small subset of resident dog cells exhibited a catabolic phenotype after dNCM+hMEPC injection accompanied by low expression of ECM markers. However, a properly balanced initial inflammatory response may contribute to tissue repair and regeneration [90] and may have favorable effects in the long-term. This is supported by a previous study which demonstrates that porcine NCM induced an initial inflammatory response, but thereafter exerted a prolonged anti-inflammatory effect [91]. The biologic role of the catabolic dog NPC subpopulation identified in this study as well as the catabolic genes expressed by the engrafted hMEPCs require validation in larger-scale follow-up studies.

The overall regenerative response of the dNCM+hMEPC treatment observed at the cellular level was further supported by a significant increase in both DNA and GAG content, potentially explained by engrafted hMEPCs producing healthy ECM, and/or a proliferative and anabolic effect of (d)NCM on the resident disc cells in line with previous studies [16-18]. Notably, an increase in DNA content was also observed in bNP explants treated with dNCM-PEG+hMEPCs. Despite the observed effects, the mode of action of dNCM+hMEPCs remains unclear, as this preliminary *in vivo* study did not observe distinct transcriptomic differences in pathway up- or downregulation in the injected disc compared with the degenerate control.

Importantly, there were no signs of a systemic immunogenic response against the xenogeneic application. Furthermore, in the absence of infiltrating immune cells, the transcriptome profiles of the subset of engrafted hMEPCs and the small subpopulation of dog NPCs in the dNCM-hMEPC treated disc used for single cell sequencing are also consistent with degenerative processes in the disc [64, 72]. From a clinical and regulatory perspective, even though we did not detect pluripotency markers in the single cell analysis, future work should focus on purification of the hMEPC population before intradiscal injection using for example the rBC2LCN lectin probe, which selectively binds to the surface of undifferentiated iPSCs [92], to mitigate the risk of tumorigenesis.

In both treated bNPs and dog NPs, we observed increased TBXT protein expression following treatment (*i.e.,* dNCM-PEG hydrogel+hMEPCs in bNPs and dNCM+hMEPCs in dog IVDs) indicating an improved NP cell phenotype. Wu *et al.* (2023) [93] demonstrated that TBXT not only marks NP identity but also actively promotes the transcription of aggrecan. Additionally, Xia *et al.* (2024) [94] provided supporting evidence showing that TBXT enhances ECM production in NPCs by stimulating SMAD3 transcription, leading to increased levels of aggrecan and collagen type II within the ECM. These findings suggests that TBXT expression may not only serve as an indicator of NC/NP-like cell identity but may also actively contribute to functional matrix production which is in line with the presence of cytoplasmatic and pericellular aggrecan in the bNPs, increased GAG content in the dog NPs after treatment, together with the preliminary evidence of functional differentiation of MEPCs into ACAN expressing cells at the gene and protein level.

The limited sequencing depth, leading to reduced detection of *e.g.* critical transcription factors, together with the small sample size, places constrains on the robustness of the conclusions. The employed study design precludes elucidation of the interplay between hMEPCs, dNCM and the resident disc cells and hence defining the mode of action. Therefore, larger scale, longer follow-up studies looking in more detail into the fate of hMEPCs after injection together with the bioactive dNCM(-PEG hydrogel) with specific attention to lineage identification at single cell level are required

to further improve the therapeutic approach based on iPSC-derived hMEPC. The present study does provide evidence that even in a xenogeneic approach hMEPCs engraft and a proportion of cells presents a functional disc cell phenotype expressing healthy ECM components like *ACAN, VCAN*, and *COL2A1*. In line with this, neurotrophin-enriched hydrogels have recently been shown to improve the efficacy of iPSC-derived brain repair and exert pronounced beneficial effects on progenitor survival and maturation [95] supporting the notion that with appropriate signaling, progenitor cells are indeed able to survive and mature further *in vivo*. As such, the concept of incorporating a tissue-specific matrisome within a hydrogel, could pave the way for bioactive material-based treatment approaches across multiple fields.

For clinical translation, it is essential to evaluate the retention of the hydrogel when exposed to long-term mechanical loading. Furthermore xenogeneic approaches, like the porcine-derived NCM conceptualized in this study, may overcome safety risks using suitable decellularization methods that remove xenogeneic DNA and minimize the potential for viral transmission. Although, the unique avascular and immune-privileged environment of the NP could facilitate clinical translation xenogeneic approaches [4, 96], immunogenic responses to xenogeneic proteins could remain an issue. The latter challenge could be addressed by identifying the key bioactive factors, elucidating their mode of action, and developing corresponding human analogs to augment the intrinsic regenerative processes.

5. Conclusions

In this study a nature-inspired conceptual bioactive hydrogel was developed using the considerable regenerative potential of dNCM by crosslinking it with PEG. The dNCM-PEG hydrogel allowed native porcine NCs to recover their phenotype and served as protective and instructive cell carrier that promotes a healthy phenotype of both injected human MEPCs and resident bovine/dog NP cells. Preliminary results indicate that the hMEPCs guided by dNCM were able to engraft and together exert anabolic effects in a preclinical dog model. We hypothesize that the increase in healthy phenotypic and ECM markers demonstrated in this study may lead to long-term regeneration and biomechanical restoration. Altogether, the presented concept of incorporating a tissue-specific matrisome within a hydrogel, underscores the potential for the application of bioactive naturally-derived and/or synthetic biomimetic biomaterials in other regenerative medicine fields.

Acknowledgments

The authors would like to thank and Adel Medzikovic and Nina van Osnabrugge (UU) for helping with the execution of the experiments and Esther Cramer (TU/e) for her support with µCT imaging and analysis. We would also like to thank the members of the iPSpine consortium for their contribution to

discussions regarding this work, especially Rebecca Williams (SHU/USFD), the group of Prof. Hans Joachim Wilke (University of Ulm) for performing the Pfirrmann grading of the discs, and the group of Prof. Danièle Noël (INSERM/IRMB) for attempting to measure Alu sequences as a measure of presence of human DNA in the limited biological material that was available. We thank Single Cell Discoveries and the FACS and single-cell core facility of the Hubrecht Institute for their assistance with the single-cell sequencing experiments and/or data analysis. Figure 1 was created using BioRender.com.

CRediT authorship contribution statement

Conceptualization: L.T.L., E.S., G.T., K.I., M.A.T., A.P., and C.L.M. **Formal analysis**: L.T.L., E.S., G.T., X.T., D.W.L., J.W., J.S., F.M.R., L.U., S.A.K., C.L.M. K.J., A.C., K.I., M.A.T, A.P., and N.S.V. **Investigation**: L.T.L., E.S., G.T., X.T., D.W.L., J.S., L.U., S.A.K, T.C.S., B.P.M., K.J., J.W., B.G., and N.S.V. **Writing - Original Draft**: L.T.L., E.S., G.T., J.W., F.M.R., S.A.K., A.C, K.J., K.I., M.A.T. **Writing - Review & Editing**: all authors. **Visualization**: L.T.L, E.S., G.T., J.W., S.A.K., J.S., L.U. **Supervision**: M.A.T., K.I., A.P., A.C., C.L.M. D.P.L, B.P.M. **Project administration**: M.A.T, K.I., A.C., B.G., C.L.M., A.P. **Funding acquisition**: M.A.T, B.G, A.C., K.I., A.P., C.L.M.

Funding

This project has received funding from the European Union's Horizon 2020 research and innovation program under grant agreement no.825925, known under the name “iPSpine” (https://ipspine.eu), the Dutch Arthritis Society (LLP22), and a research grant from Research Ireland through Grant number 13/RC/2073_2.

Declaration of competing interest

Keita Ito and Tara C. Schmitz report a relationship with NC Biomatrix that includes: CSO and Senior Scientific Consultant respectively of NC Biomatrix, a company developing dNCM as a commercial product, which holds a license to the IP for its production process [United States Patent Application 20190022278]. The other authors declare that they have no known competing financial interests or personal relationships that could have appeared to influence the work reported in this paper.

Data availability

The scRNA-Seq datasets generated and analyzed during this study will be deposited in the NCBI Gene Expression Omnibus (GEO) repository.

References

[1] K. Luoma, H. Riihimäki, R. Luukkonen, R. Raininko, E. Viikari-Juntura, A. Lamminen, Low back pain in relation to lumbar disc degeneration, Spine 25(4) (2000) 487–492.

[2] K.M. Cheung, D. Samartzis, J. Karppinen, K.D. Luk, Are "patterns" of lumbar disc degeneration associated with low back pain?: new insights based on skipped level disc pathology, Spine (Phila Pa 1976) 37(7) (2012) E430–8.

[3] M.A. Adams, P.J. Roughley, What is intervertebral disc degeneration, and what causes it?, Spine 31(18) (2006) 2151–2161.

[4] J.P. Urban, S. Smith, J.C. Fairbank, Nutrition of the intervertebral disc, Spine (Phila Pa 1976) 29(23) (2004) 2700–9.

[5] A.A. Thorpe, F.C. Bach, M.A. Tryfonidou, C.L. Le Maitre, F. Mwale, A.D. Diwan, K. Ito, Leaping the hurdles in developing regenerative treatments for the intervertebral disc from preclinical to clinical, JOR Spine 1(3) (2018) e1027.

[6] E. Salzer, V.H.M. Mouser, J.A. Bulsink, M.A. Tryfonidou, K. Ito, Dynamic loading leads to increased metabolic activity and spatial redistribution of viable cell density in nucleus pulposus tissue, JOR Spine 6(1) (2023) e1240.

[7] J. Schol, D. Sakai, Comprehensive narrative review on the analysis of outcomes from cell transplantation clinical trials for discogenic low back pain, North American Spine Society Journal (NASSJ) 13 (2023) 100195.

[8] Y.-M. Pers, R. Soler-Rich, G. Vadalà, R. Ferreira, C. Duflos, M.-C. Picot, F. Herman, S. Broussous, A. Sánchez, D. Noriega, Allogenic bone marrow–derived mesenchymal stromal cell–based therapy for patients with chronic low back pain: a prospective, multicentre, randomised placebo controlled trial (RESPINE study), Annals of the Rheumatic Diseases 83(11) (2024) 1572–1583.

[9] M.V. Risbud, Z.R. Schoepflin, F. Mwale, R.A. Kandel, S. Grad, J.C. Iatridis, D. Sakai, J.A. Hoyland, Defining the phenotype of young healthy nucleus pulposus cells: recommendations of the Spine Research Interest Group at the 2014 annual ORS meeting, J Orthop Res 33(3) (2015) 283–93.

[10] F.C. Bach, D.W. Poramba-Liyanage, F.M. Riemers, J. Guicheux, A. Camus, J.C. Iatridis, D. Chan, K. Ito, C.L. Le Maitre, M.A. Tryfonidou, Notochordal Cell-Based Treatment Strategies and Their Potential in Intervertebral Disc Regeneration, Front Cell Dev Biol 9 (2021) 780749.

[11] C.J. Hunter, J.R. Matyas, N.A. Duncan, The notochordal cell in the nucleus pulposus: a review in the context of tissue engineering, Tissue Eng 9(4) (2003) 667–77.

[12] T. Liebscher, M. Haefeli, K. Wuertz, A.G. Nerlich, N. Boos, Age-related variation in cell density of human lumbar intervertebral disc, Spine 36(2) (2011) 153–159.

[13] T. Miyazaki, S. Kobayashi, K. Takeno, A. Meir, J. Urban, H. Baba, A phenotypic comparison of proteoglycan production of intervertebral disc cells isolated from rats, rabbits, and bovine tails; which animal model is most suitable to study tissue engineering and biological repair of human disc disorders?, Tissue Eng Part A 15(12) (2009) 3835–46.

[14] R. Cappello, J.L. Bird, D. Pfeiffer, M.T. Bayliss, J. Dudhia, Notochordal cell produce and assemble extracellular matrix in a distinct manner, which may be responsible for the maintenance of healthy nucleus pulposus, Spine (Phila Pa 1976) 31(8) (2006) 873–82; discussion 883.

[15] F. Bach, S. Libregts, L. Creemers, B. Meij, K. Ito, M. Wauben, M. Tryfonidou, Notochordal-cell derived extracellular vesicles exert regenerative effects on canine and human nucleus pulposus cells, Oncotarget 8(51) (2017) 88845–88856.

[16] T.C. Schmitz, M. van Doeselaar, M.A. Tryfonidou, K. Ito, Detergent-Free Decellularization of Notochordal Cell-Derived Matrix Yields a Regenerative, Injectable, and Swellable Biomaterial, ACS Biomater Sci Eng 8(9) (2022) 3912–3923.

[17] F.C. Bach, A.R. Tellegen, M. Beukers, A. Miranda-Bedate, M. Teunissen, W.A.M. de Jong, S.A.H. de Vries, L.B. Creemers, K. Benz, B.P. Meij, K. Ito, M.A. Tryfonidou, Biologic canine and human intervertebral disc repair by notochordal cell-derived matrix: from bench towards bedside, Oncotarget 9(41) (2018) 26507–26526.

[18] S. de Vries, M.V. Doeselaar, B. Meij, M. Tryfonidou, K. Ito, Notochordal Cell Matrix As a Therapeutic Agent for Intervertebral Disc Regeneration, Tissue Eng Part A 25(11-12) (2019) 830–841.

[19] E. Gruskin, B.A. Doll, F.W. Futrell, J.P. Schmitz, J.O. Hollinger, Demineralized bone matrix in bone repair: history and use, Advanced drug delivery reviews 64(12) (2012) 1063–1077.

[20] W.G. de, R.L. Berghmans, G.J. Boer, S. Andersen, B. Brambati, A.S. Carvalho, K. Dierickx, S. Elliston, P. Nunez, W. Osswald, M. Vicari, Ethical guidance on human embryonic and fetal tissue transplantation: a European overview, Med Health Care Philos 5(1) (2002) 79–90.

[21] Y.-J. Peng, X. Huang, Q. Zhou, Ethical and policy considerations for human embryo and stem cell research in China, Cell Stem Cell 27(4) (2020) 511–514.

[22] R.J. Williams, L.T. Laagland, F.C. Bach, L. Ward, W. Chan, V. Tam, A. Medzikovic, S. Basatvat, L. Paillat, N. Vedrenne, J.W. Snuggs, D.W. Poramba-Liyanage, J.A. Hoyland, D. Chan, A. Camus, S.M. Richardson, M.A. Tryfonidou, C.L. Le Maitre, Recommendations for intervertebral disc notochordal cell investigation: From isolation to characterization, JOR Spine 6(3) (2023) e1272.
[23] R.J. Williams, M.A. Tryfonidou, J.W. Snuggs, C.L. Le Maitre, Cell sources proposed for nucleus pulposus regeneration, JOR Spine 4(4) (2021) e1175.
[24] J. Warin, N. Vedrenne, V. Tam, M. Zhu, D. Yin, X. Lin, B. Guidoux-D'halluin, A. Humeau, L. Roseiro, L. Paillat, C. Chedeville, C. Chariau, F. Riemers, M. Templin, J. Guicheux, M.A. Tryfonidou, J.W.K. Ho, L. David, D. Chan, A. Camus, In vitro and in vivo models define a molecular signature reference for human embryonic notochordal cells, iScience 27(2) (2024) 109018.
[25] P. Colombier, B. Halgand, C. Chedeville, C. Chariau, V. Francois-Campion, S. Kilens, N. Vedrenne, J. Clouet, L. David, J. Guicheux, A. Camus, NOTO Transcription Factor Directs Human Induced Pluripotent Stem Cell-Derived Mesendoderm Progenitors to a Notochordal Fate, Cells 9(2) (2020).
[26] R. Tang, L. Jing, V.P. Willard, C.L. Wu, F. Guilak, J. Chen, L.A. Setton, Differentiation of human induced pluripotent stem cells into nucleus pulposus-like cells, Stem Cell Res Ther 9(1) (2018) 61.
[27] Y. Zhang, Z. Zhang, P. Chen, C.Y. Ma, C. Li, T.Y.K. Au, V. Tam, Y. Peng, R. Wu, K.M.C. Cheung, P.C. Sham, H.F. Tse, D. Chan, V.Y. Leung, K.S.E. Cheah, Q. Lian, Directed Differentiation of Notochord-like and Nucleus Pulposus-like Cells Using Human Pluripotent Stem Cells, Cell Rep 30(8) (2020) 2791–2806 e5.
[28] M.E. Diaz-Hernandez, N.M. Khan, C.M. Trochez, T. Yoon, P. Maye, S.M. Presciutti, G. Gibson, H. Drissi, Derivation of notochordal cells from human embryonic stem cells reveals unique regulatory networks by single cell-transcriptomics, Journal of cellular physiology 235(6) (2020) 5241–5255.
[29] K. Joyce, G.T. Fabra, Y. Bozkurt, A. Pandit, Bioactive potential of natural biomaterials: Identification, retention and assessment of biological properties, Signal transduction and targeted therapy 6(1) (2021) 122.
[30] Z. Liu, Z. Zheng, J. Qi, J. Wang, Q. Zhou, F. Hu, J. Liang, C. Li, W. Zhang, X. Zhang, CD24 identifies nucleus pulposus progenitors/notochordal cells for disc regeneration, Journal of Biological Engineering 12 (2018) 1–15.
[31] J. Chen, E.J. Lee, L. Jing, N. Christoforou, K.W. Leong, L.A. Setton, Differentiation of mouse induced pluripotent stem cells (iPSCs) into nucleus pulposus-like cells in vitro, PLoS One 8(9) (2013) e75548.
[32] C.J. Panebianco, J.H. Meyers, J. Gansau, W.W. Hom, J.C. Iatridis, Balancing biological and biomechanical performance in intervertebral disc repair: a systematic review of injectable cell delivery biomaterials, Eur Cell Mater 40 (2020) 239–258.
[33] M. Alini, S.M. Eisenstein, K. Ito, C. Little, A.A. Kettler, K. Masuda, J. Melrose, J. Ralphs, I. Stokes, H.J. Wilke, Are animal models useful for studying human disc disorders/degeneration?, Eur Spine J 17(1) (2008) 2–19.
[34] N.N. Lee, E. Salzer, F.C. Bach, A.F. Bonilla, J.L. Cook, Z. Gazit, S. Grad, K. Ito, L.J. Smith, A. Vernengo, H.J. Wilke, J.B. Engiles, M.A. Tryfonidou, A comprehensive tool box for large animal studies of intervertebral disc degeneration, JOR Spine 4(2) (2021) e1162.
[35] F. Causa, L. Manto, A. Borzacchiello, R. De Santis, P.A. Netti, L. Ambrosio, L. Nicolais, Spatial and structural dependence of mechanical properties of porcine intervertebral disc, J Mater Sci Mater Med 13(12) (2002) 1277–80.
[36] E. Salzer, V.H.M. Mouser, M.A. Tryfonidou, K. Ito, A bovine nucleus pulposus explant culture model, J Orthop Res 40(9) (2022) 2089–2102.
[37] M. Fusellier, J. Clouet, O. Gauthier, M. Tryfonidou, C. Le Visage, J. Guicheux, Degenerative lumbar disc disease: in vivo data support the rationale for the selection of appropriate animal models, Eur Cell Mater 39 (2020) 18–47.
[38] E. Salzer, T.C. Schmitz, V.H. Mouser, A. Vernengo, B. Gantenbein, J.U. Jansen, C. Neidlinger-Wilke, H.J. Wilke, S. Grad, C.L. Le Maitre, M.A. Tryfonidou, K. Ito, Ex vivo intervertebral disc cultures: degeneration-induction methods and their implications for clinical translation, Eur Cell Mater 45 (2023) 88–112.
[39] N. Willems, G. Mihov, G.C. Grinwis, M. van Dijk, D. Schumann, C. Bos, G.J. Strijkers, W.J. Dhert, B.P. Meij, L.B. Creemers, Safety of intradiscal injection and biocompatibility of polyester amide (PEA) microspheres in a canine model predisposed to intervertebral disc degeneration, Regenerative therapies for intervertebral disc degeneration (2016) 43.
[40] S. Basatvat, F.C. Bach, M.N. Barcellona, A.L. Binch, C.T. Buckley, B. Bueno, N.O. Chahine, A. Chee, L.B. Creemers, S. Dudli, B. Fearing, S.J. Ferguson, J. Gansau, B. Gantenbein, R. Gawri, J.D. Glaeser, S. Grad, J. Guerrero, L. Haglund, P.A. Hernandez, J.A. Hoyland, C. Huang, J.C. Iatridis, S. Illien-Junger, L. Jing, P. Kraus, L.T. Laagland, G. Lang, V. Leung, Z. Li, T. Lufkin, J.C. van Maanen, E.E. McDonnell, C.J. Panebianco, S.M. Presciutti, S. Rao, S.M. Richardson, S. Romereim, T.C. Schmitz, J. Schol, L. Setton, D. Sheyn, J.W. Snuggs, Y. Sun, X. Tan, M.A. Tryfonidou, N. Vo, D. Wang, B. Williams, R. Williams, S.T. Yoon, C.L. Le Maitre, Harmonization and standardization of nucleus pulposus cell extraction and culture methods, JOR Spine 6(1) (2023) e1238.

[41] S.H. Yang, M.H. Hu, Y.H. Sun, F.H. Lin, Differential phenotypic behaviors of human degenerative nucleus pulposus cells under normoxic and hypoxic conditions: influence of oxygen concentration during isolation, expansion, and cultivation, Spine J 13(11) (2013) 1590–6.
[42] J. Snuggs, S. Basatvat, E. Kanelis, A. Binch, L. Alexopoulos, M.A. Tryfonidou, C.L. Le Maitre, Understanding the physiological behaviour of disc cells in an in vitro imitation of the healthy and degenerated disc niche, (2025) (manuscript submitted).
[43] P.-A. Faye, N. Vedrenne, F. Miressi, M. Rassat, S. Romanenko, L. Richard, S. Bourthoumieu, B. Funalot, F. Sturtz, F. Favreau, Optimized protocol to generate spinal motor neuron cells from induced pluripotent stem cells from Charcot Marie Tooth patients, Brain Sciences 10(7) (2020) 407.
[44] S. Kilens, D. Meistermann, D. Moreno, C. Chariau, A. Gaignerie, A. Reignier, Y. Lelievre, M. Casanova, C. Vallot, S. Nedellec, L. Flippe, J. Firmin, J. Song, E. Charpentier, J. Lammers, A. Donnart, N. Marec, W. Deb, A. Bihouee, C. Le Caignec, C. Pecqueur, R. Redon, P. Barriere, J. Bourdon, V. Pasque, M. Soumillon, T.S. Mikkelsen, C. Rougeulle, T. Freour, L. David, C. Milieu Interieur, Parallel derivation of isogenic human primed and naive induced pluripotent stem cells, Nat Commun 9(1) (2018) 360.
[45] I.T. Arkesteijn, V.H. Mouser, F. Mwale, B.G. van Dijk, K. Ito, A Well-Controlled Nucleus Pulposus Tissue Culture System with Injection Port for Evaluating Regenerative Therapies, Ann Biomed Eng 44(5) (2016) 1798–807.
[46] S. Kobayashi, H. Baba, K. Takeno, T. Miyazaki, A. Meir, J. Urban, Physical limitations to tissue engineering of intervertabral disc cells, Tissue Engineering (2010) 247–281.
[47] C.H. Hulme, M. Westwood, J.E. Myers, A.E. Heazell, A high-throughput colorimetric-assay for monitoring glucose consumption by cultured trophoblast cells and placental tissue, Placenta 33(11) (2012) 949–51.
[48] J.C. Salvatierra, T.Y. Yuan, H. Fernando, A. Castillo, W.Y. Gu, H.S. Cheung, C.Y. Huant, Difference in Energy Metabolism of Annulus Fibrosus and Nucleus Pulposus Cells of the Intervertebral Disc, Cell Mol Bioeng 4(2) (2011) 302–310.
[49] Y.J. Kim, R.L. Sah, J.Y. Doong, A.J. Grodzinsky, Fluorometric assay of DNA in cartilage explants using Hoechst 33258, Anal Biochem 174(1) (1988) 168–76.
[50] L. Creemers, D. Jansen, A. van Veen-Reurings, T. Van Den Bos, V. Everts, Microassay for the assessment of low levels of hydroxyproline, Biotechniques 22(4) (1997) 656–658.
[51] R.E. Neuman, M.A. Logan, The determination of hydroxyproline, J Biol Chem 184(1) (1950) 299–306.
[52] X. Tong, D.W. Poramba-Liyanage, M. van Hoolwerff, F.M. Riemers, J. Montilla-Rojo, J. Warin, D. Salvatori, A. Camus, I. Meulenbelt, Y.F.M. Ramos, N. Geijssen, M.A. Tryfonidou, P. Shang, Prospective Isolation and Tracing of Matrix-Producing Notochordal and Chondrocyte Cells using Aggrecan-2A-mScarlet Reporter Lines from Human iPSCs, Science Advances (2024).
[53] M. Muraro, G. Dharmadhikari, D. Grün, N. Groen, T. Dielen, E. Jansen, L. van Gurp, M. Engelse, F. Carlotti, E. de Koning, A single-cell transcriptome atlas of the human pancreas. Cell Syst. 3, 385–394. e3, 2016.
[54] Y. Hao, T. Stuart, M.H. Kowalski, S. Choudhary, P. Hoffman, A. Hartman, A. Srivastava, G. Molla, S. Madad, C. Fernandez-Granda, Dictionary learning for integrative, multimodal and scalable single-cell analysis, Nature biotechnology 42(2) (2024) 293–304.
[55] S. Choudhary, R. Satija, Comparison and evaluation of statistical error models for scRNA-seq, Genome biology 23(1) (2022) 27.
[56] X. Tong, D.W. Poramba-Liyanage, M. van Hoolwerff, F.M. Riemers, J. Montilla-Rojo, J. Warin, D. Salvatori, A. Camus, I. Meulenbelt, Y.F. Ramos, Isolation and tracing of matrix-producing notochordal and chondrocyte cells using ACAN-2A-mScarlet reporter human iPSC lines, Science advances 10(43) (2024) eadp3170.
[57] G.W. Omlor, A.G. Nerlich, U.K. Tirlapur, J.P. Urban, T. Guehring, Loss of notochordal cell phenotype in 3D-cell cultures: implications for disc physiology and disc repair, Arch Orthop Trauma Surg 134(12) (2014) 1673–81.
[58] T.C. Schmitz, B. van Genabeek, M.J. Pouderoijen, H.M. Janssen, M. van Doeselaar, J.F. Crispim, M.A. Tryfonidou, K. Ito, Semi-synthetic degradable notochordal cell-derived matrix hydrogel for use in degenerated intervertebral discs: Initial in vitro characterization, J Biomed Mater Res A 111(12) (2023) 1903–1915.
[59] A. Tellegen, I. Rudnik-Jansen, M. Beukers, A. Miranda-Bedate, F. Bach, W. De Jong, N. Woike, G. Mihov, J. Thies, B. Meij, Intradiscal delivery of celecoxib-loaded microspheres restores intervertebral disc integrity in a preclinical canine model, Journal of Controlled Release 286 (2018) 439–450.
[60] A.R. Tellegen, I. Rudnik-Jansen, M. Beukers, A. Miranda-Bedate, F.C. Bach, W. de Jong, N. Woike, G. Mihov, J.C. Thies, B.P. Meij, L.B. Creemers, M.A. Tryfonidou, Intradiscal delivery of celecoxib-loaded microspheres restores intervertebral disc integrity in a preclinical canine model, J Control Release 286 (2018) 439–450.
[61] Y. Xu, Z. Xie, S. Gu, X. Zhao, D. Zhao, Z. Wu, J. Wang, T. Xu, R. Xu, Z. Feng, Fibro-NPC: a pathogenic subtype identified at single-cell resolution with secreted SFRP4 as a biomarker in intervertebral disc degeneration, Journal of Translational Medicine 23(1) (2025) 867.

[62] C. Zhang, L. Zhong, Y.K. Lau, M. Wu, L. Yao, T.P. Schaer, R.L. Mauck, N.R. Malhotra, L. Qin, L.J. Smith, Single cell RNA sequencing reveals emergent notochord-derived cell subpopulations in the postnatal nucleus pulposus, FASEB journal: official publication of the Federation of American Societies for Experimental Biology 38(1) (2024) e23363.
[63] T. Zhou, Y. Chen, Z. Liao, L. Zhang, D. Su, Z. Li, X. Yang, X. Ke, H. Liu, Y. Chen, Spatiotemporal characterization of human early intervertebral disc formation at single-cell resolution, Advanced Science 10(14) (2023) 2206296.
[64] M.V. Risbud, I.M. Shapiro, Role of cytokines in intervertebral disc degeneration: pain and disc content, Nature Reviews Rheumatology 10(1) (2014) 44–56.
[65] K. Wuertz, L. Haglund, Inflammatory mediators in intervertebral disk degeneration and discogenic pain, Global spine journal 3(3) (2013) 175–184.
[66] V. Tam, P. Chen, A. Yee, N. Solis, T. Klein, M. Kudelko, R. Sharma, W.C. Chan, C.M. Overall, L. Haglund, DIPPER, a spatiotemporal proteomics atlas of human intervertebral discs for exploring ageing and degeneration dynamics, Elife 9 (2020) e64940.
[67] Z. Wang, D. Zhu, F. Yang, H. Chen, J. Kang, W. Liu, A. Lin, X. Kang, POSTN knockdown suppresses IL-1β-induced inflammation and apoptosis of nucleus pulposus cells via inhibiting the NF-κB pathway and alleviates intervertebral disc degeneration, Journal of Cell Communication and Signaling 18(2) (2024) e12030.
[68] S. Rajasekaran, D.C.R. Soundararajan, S.M. Nayagam, C. Tangavel, M. Raveendran, K.S.V. Anand, A.P. Shetty, R.M. Kanna, Novel biomarkers of health and degeneration in human intervertebral discs: in-depth proteomic analysis of collagen framework of fetal, healthy, scoliotic, degenerate, and herniated discs, Asian Spine Journal 17(1) (2022) 17.
[69] D. Li, J. Yue, L. Jiang, Y. Huang, J. Sun, Y. Wu, Correlation between expression of high temperature requirement serine protease A1 (HtrA1) in nucleus pulposus and T2 value of magnetic resonance imaging, Medical Science Monitor: International Medical Journal of Experimental and Clinical Research 23 (2017) 1940.
[70] R. Wang, C. Xu, H. Zhong, B. Hu, L. Wei, N. Liu, Y. Zhang, Q. Shi, C. Wang, M. Qi, Inflammatory-sensitive CHI3L1 protects nucleus pulposus via AKT3 signaling during intervertebral disc degeneration, The FASEB Journal 34(3) (2020) 3554–3569.
[71] D. W. Poramba-Liyanage, X. Tong, F. M. Riemers, B. P. Meij, Y. Dilek, C.G.J. Cleypool, S. Kamali, Christine L. Le Maitre, A. Camus, D. Chan, A. van Oudenaarden, P. Zeller, M.A. Tryfonidou, Removal of H3K27me3 histone modification as therapy for intervertebral disc degeneration: discovery via single-cell multi-omics, (2025) (manuscript submitted).
[72] K. Wuertz, L. Haglund, Inflammatory mediators in intervertebral disk degeneration and discogenic pain, Global Spine J 3(3) (2013) 175–84.
[73] R. Ali, C. Le Maitre, S. Richardson, J. Hoyland, A. Freemont, Connective tissue growth factor expression in human intervertebral disc: implications for angiogenesis in intervertebral disc degeneration, Biotechnic & Histochemistry 83(5) (2008) 239–245.
[74] K. Wang, W. Liu, Y. Song, X. Wu, Y. Zhang, S. Li, Y. Gao, J. Tu, Y. Liu, C. Yang, The role of angiopoietin-2 in nucleus pulposus cells during human intervertebral disc degeneration, Laboratory Investigation 97(8) (2017) 971–982.
[75] S.H. Peck, K.K. McKee, J.W. Tobias, N.R. Malhotra, B.D. Harfe, L.J. Smith, Whole transcriptome analysis of notochord-derived cells during embryonic formation of the nucleus pulposus, Scientific reports 7(1) (2017) 10504.
[76] J.M. Cloyd, N.R. Malhotra, L. Weng, W. Chen, R.L. Mauck, D.M. Elliott, Material properties in unconfined compression of human nucleus pulposus, injectable hyaluronic acid-based hydrogels and tissue engineering scaffolds, Eur Spine J 16(11) (2007) 1892–8.
[77] N. Zerbinati, C. Esposito, G. Cipolla, A. Calligaro, D. Monticelli, V. Martina, M. Golubovic, I. Binic, J. Sigova, A.L. Gallo, Chemical and mechanical characterization of hyaluronic acid hydrogel cross-linked with polyethylen glycol and its use in dermatology, Dermatologic Therapy 33(4) (2020) e13747.
[78] Y. Navaro, N. Bleich-Kimelman, L. Hazanov, I. Mironi-Harpaz, Y. Shachaf, S. Garty, Y. Smith, G. Pelled, D. Gazit, D. Seliktar, Z. Gazit, Matrix stiffness determines the fate of nucleus pulposus-derived stem cells, Biomaterials 49 (2015) 68–76.
[79] J.Y. Wang, A.E. Baer, V.B. Kraus, L.A. Setton, Intervertebral disc cells exhibit differences in gene expression in alginate and monolayer culture, Spine (Phila Pa 1976) 26(16) (2001) 1747–51; discussion 1752.
[80] A. Rastogi, P. Thakore, A. Leung, M. Benavides, M. Machado, M.A. Morschauser, A.H. Hsieh, Environmental regulation of notochordal gene expression in nucleus pulposus cells, J Cell Physiol 220(3) (2009) 698–705.
[81] B. Gantenbein, E. Calandriello, K. Wuertz-Kozak, L.M. Benneker, M.J. Keel, S.C. Chan, Activation of intervertebral disc cells by co-culture with notochordal cells, conditioned medium and hypoxia, BMC Musculoskelet Disord 15 (2014) 422.

[82] E. Potier, K. Ito, Using notochordal cells of developmental origin to stimulate nucleus pulposus cells and bone marrow stromal cells for intervertebral disc regeneration, Eur Spine J 23(3) (2014) 679–88.
[83] S. Spillekom, L.A. Smolders, G.C. Grinwis, I.T. Arkesteijn, K. Ito, B.P. Meij, M.A. Tryfonidou, Increased osmolarity and cell clustering preserve canine notochordal cell phenotype in culture, Tissue Eng Part C Methods 20(8) (2014) 652–62.
[84] I.T. Arkesteijn, L.A. Smolders, S. Spillekom, F.M. Riemers, E. Potier, B.P. Meij, K. Ito, M.A. Tryfonidou, Effect of coculturing canine notochordal, nucleus pulposus and mesenchymal stromal cells for intervertebral disc regeneration, Arthritis Res Ther 17(1) (2015) 60.
[85] R. Williams, S. Basatvat, T. Schmitz, R. Janani, C. Sammon, K. Benz, K. Ito, M. Tryfonidou, J. Snuggs, C. Le Maitre, Potential of notochordal cells within injectable biomaterials to promote intervertebral disc regeneration, European Cells and Materials 47 (2024) 30–50.
[86] L. Paillat, K. Coutant, M. Dutilleul, S. Le Lay, A. Camus, Three-dimensional culture model to study the biology of vacuolated notochordal cells from mouse nucleus pulposus explants, Eur Cell Mater 45 (2023) 72–87.
[87] L.T. Laagland, D.W. Poramba Liyanage, R. Desprat, F.M. Riemers, C.C. Warmerdam, M. Soubeyrand, P. Bensadoun, K. Ito, O. Milhavet, A. Camus, Disc-Derived Induced Pluripotent Stem Cells and Environmental Cues for Nucleus Pulposus Regeneration, Tissue Engineering Part A (2025).
[88] H. Choi, Z. I Johnson, M. V Risbud, Understanding nucleus pulposus cell phenotype: a prerequisite for stem cell based therapies to treat intervertebral disc degeneration, Current stem cell research & therapy 10(4) (2015) 307–316.
[89] W. Jiang, J.D. Glaeser, K. Salehi, G. Kaneda, P. Mathkar, A. Wagner, R. Ho, D. Sheyn, Single-cell atlas unveils cellular heterogeneity and novel markers in human neonatal and adult intervertebral discs, Iscience 25(7) (2022).
[90] M. Molinos, C.R. Almeida, J. Caldeira, C. Cunha, R.M. Gonçalves, M.A. Barbosa, Inflammation in intervertebral disc degeneration and regeneration, Journal of the Royal Society Interface 12(104) (2015) 20141191.
[91] L. Laagland, F. Bach, F. Riemers, G. Erdmann, T. Braun, G. van den Akker, T. Schmitz, L. Creemers, C. Sachse, C. Le Maitre, Notochordal cell-derived matrix inhibits MAPK signaling in the degenerative disc environment, European Cells and Materials 46 (2023) 57–90.
[92] Y. Haramoto, Y. Onuma, S. Mawaribuchi, Y. Nakajima, Y. Aiki, K. Higuchi, M. Shimizu, H. Tateno, J. Hirabayashi, Y. Ito, A technique for removing tumourigenic pluripotent stem cells using rBC2LCN lectin, Regenerative therapy 14 (2020) 306–314.
[93] Y. Wu, Y. Xia, C. Yue, T. Xin, Q. Wang, H. Zhang, C. Shen, M. Shen, Y. Gu, J. Shen, Brachyury positively regulates extracellular matrix synthesis via directly promoting aggrecan transcription in nucleus pulposus, FASEB J 37(6) (2023) e22976.
[94] Y. Xia, Y. Wu, Y. Gong, C. Yue, L. Tao, T. Xin, C. Shen, Y. Zhu, M. Shen, J. Shen, Brachyury promotes extracellular matrix synthesis through transcriptional regulation of Smad3 in nucleus pulposus, American Journal of Physiology-Cell Physiology 326(5) (2024) C1384–C1397.
[95] G. Comini, R. Kelly, S. Jarrin, T. Patton, K. Narasimhan, A. Pandit, N. Drummond, T. Kunath, E. Dowd, Survival and maturation of human induced pluripotent stem cell-derived dopaminergic progenitors in the parkinsonian rat brain is enhanced by transplantation in a neurotrophin-enriched hydrogel, J Neural Eng 21(2) (2024).
[96] T. Takada, K. Nishida, M. Doita, M. Kurosaka, Fas ligand exists on intervertebral disc cells: a potential molecular mechanism for immune privilege of the disc, Spine (Phila Pa 1976) 27(14) (2002) 1526–30.